

A Poisson-Nernst-Planck single ion channel model and its effective finite element solver

Dexuan Xie^{a,*}, Zhen Chao^b

^a Department of Mathematical Sciences, University of Wisconsin-Milwaukee, Milwaukee, WI 53201, USA

^b Department of Mathematics, University of Michigan, Ann Arbor, MI 48109, USA



ARTICLE INFO

Article history:

Received 22 October 2022

Received in revised form 30 January 2023

Accepted 27 February 2023

Available online 5 March 2023

Keywords:

Poisson-Nernst-Planck equations

Finite element method

Single ion channel

Potassium channel

Electric current calculation

ABSTRACT

A single ion channel is a membrane protein with an ion selectivity filter that allows only a single species of ions (such as potassium ions) to pass through in the “open” state. Its selectivity filter also naturally separates a solvent domain into an intracellular domain and an extracellular domain. Such biological and geometrical characteristics of a single ion channel are novelly adopted in the construction of a new kind of dielectric continuum ion channel model, called the Poisson-Nernst-Planck single ion channel (PNPSIC) model, in this paper. An effective PNPSIC finite element solver is then developed and implemented as a software package workable for a single ion channel with a three-dimensional X-ray crystallographic molecular structure and a mixture of multiple ionic species. Numerical results for a potassium channel confirm the convergence and efficiency of the PNPSIC finite element solver and demonstrate the high performance of the software package. Moreover, the PNPSIC model is applied to the calculation of electric current and validated by biophysical experimental data.

© 2023 Elsevier Inc. All rights reserved.

1. Introduction

A system of Poisson-Nernst-Planck (PNP) equations is a basic tool for the development of dielectric continuum ion channel models. In the last three years, we developed several PNP ion channel (PNPic) models using novel boundary value and interface conditions and membrane surface charge densities to reflect real membrane environments, along with their finite element solvers and software packages, which are workable for a crystallographic three-dimensional (3D) molecular structure of an ion channel protein and a mixture of multiple ionic species [1–3]. We also have significantly improved an ion channel tetrahedral mesh generation software package to generate high-quality tetrahedral meshes for our PNP finite element solvers [4]. These models and software packages have been applied to the calculation of membrane kinetics such as membrane potentials, transport fluxes, and electric currents, making them valuable in the simulation of either a non-selective cation channel such as a gramicidin A [5], which allows multiple types of cations through the channel, or a voltage-dependent anion channel, which is the main conduit for different ions and metabolites into and out of a mitochondrion [6]. However, like other PNP ion channel models, our PNPic models do not work for a single ion channel — a membrane protein with an ion selectivity filter that only allows one species of ions to pass across a membrane in its “open” state.

* Corresponding author.

E-mail address: dxie@uwm.edu (D. Xie).

Typically, single ion channels can be classified into potassium channels, sodium channels, calcium channels, chloride channels, and proton channels [7]. They are found in the cellular membranes of virtually all living organisms, playing essential roles in coordinating contraction in the heart and skeletal muscle, controlling electrical activity in cells, and producing signals of the nervous system [7,8]. Among them, potassium channels are the most widely studied by molecular dynamics [9–15] and Brownian dynamics [16,17] due to the availability of high-quality X-ray crystallographic structural data [18–20]. However, either molecular dynamics or Brownian dynamics can be much more costly than PNP equations in the calculation of membrane kinetics since PNP equations not only treat the water solvent as a dielectric continuum medium based on the implicit solvent approach but also describe ionic distributions in continuous concentration functions based on the mean-field approach [21,22]. Thus, a lot of research work was also done toward the direction of developing PNP ion channel models [23]. Note that a PNP ion channel model cannot distinguish the two ions with the same charge, such as sodium and potassium ions, since it treats ions as volume less points. Hence, several size modified PNP and Poisson-Boltzmann models have been developed to reflect various ion size effects [24–30]. Unfortunately, they still do not work for a potassium channel because the selectivity filter of a potassium channel prefers larger potassium ions to smaller sodium ions. Such an unconventional ion selectivity behavior contradicts the physical law of momentum, under which, a sodium ion should be a stronger biological competitor to fight for space in the selectivity filter than a potassium ion since all the ions are assumed to have the same mass density in PNP equations. This fascinating phenomenon has motivated researchers to further modify Nernst-Planck equations by adding an additional solvation energy. For example, a Born solvation energy is selected to construct a PNP single ion channel model, called the Born-energy modified PNP model, in [31] since sodium ions are observed to have larger Born solvation energy values than potassium ions. Similarly, a one-dimensional solvation energy modified PNP ion channel model is developed in [32]. These two models were shown numerically to be able to select potassium ions over sodium ions.

In this work, we develop a novel PNP single ion channel (PNPSIC) model according to the biological and geometrical characteristics of a single ion channel. In fact, in a current PNP ion channel model, all the ions have been assumed to be able to enter the selectivity filter since all the ionic concentrations are defined in a solvent domain, D_s . Clearly, such a hypothesis contradicts with the single ion selectivity property, which causes either the failure of the current PNP ion channel model or the difficulties of modifying the current PNP ion channel model for a single ion channel case. We observe that actually, a solvent domain, D_s , has been separated by the selectivity filter into an intracellular domain, $D_{s,i}$, and an extracellular domain, $D_{s,e}$. Since the ions of the single ionic species are the only ions that can transport between $D_{s,i}$ and $D_{s,e}$ through the selectivity filter, for a mixture of n ionic species, we can describe the ionic distributions of a single ion channel in terms of $2n - 1$ concentration functions – a set of $n - 1$ concentration functions defined in $D_{s,i}$, another set of $n - 1$ concentration functions in $D_{s,e}$, and a concentration function of the single species in D_s . To define these $2n - 1$ concentration functions, we need to construct $2n - 1$ boundary value problems and we can do so using classical Nernst-Planck equations. With these concentration functions, we then use Poisson equations to construct a boundary value problem for defining an electrostatic potential function in a simulation box domain, Ω , which consists of D_s , an ion channel protein region, and a membrane region. A combination of these $2n$ boundary value problems leads to a nonlinear system as the definition of our PNPSIC model.

One advantage of the PNPSIC model is to let us block all the other ions to enter the filter easily in comparison with a corresponding Born-energy modified PNP model. However, the PNPSIC model is more challenging to solve numerically because it involves more complicated physical domains and more unknown functions while it faces the same numerical difficulties caused by potential function singularities and positive sign restrictions on concentration functions as the PNP ion channel model does. Based on our current PNP ion channel work [1–3], we develop mathematical and numerical techniques to overcome these difficulties. We also develop a finite element method for solving the PNPSIC model since with a finite element method, we can approximate the geometrical shapes of the complex interfaces of the box domain Ω and the complex domains $D_{s,i}$, $D_{s,e}$, and D_s through properly constructing irregular tetrahedral meshes in a much higher degree of accuracy than the corresponding finite difference or finite volume method. Indeed, it is critical to retain the geometrical shapes of $D_{s,i}$, $D_{s,e}$, D_s , and the interfaces since the geometrical shapes can seriously affect not only the biological properties of an ion channel protein but also the solution properties of the PNPSIC model. However, the selectivity filter has a very narrow open pore. For example, the selectivity filter pore of a potassium channel has an average radius of 1.4 Å only [18]. Thus, generating such tetrahedral meshes is challenging and requires us to further improve the current ion channel mesh software package. This turns out to be one key step for us to develop a PNPSIC finite element solver. We have completed this mesh work and plan to report it in another paper due to its length in description.

In this work, we report an effective PNPSIC finite element iterative scheme and a related software package for a single ion channel protein with a three-dimensional crystallographic molecular structure and a mixture of multiple ionic species. Numerical experiments are then reported for a potassium channel to confirm the convergence and efficiency of the iterative scheme, to demonstrate the performance of the software package, and to validate our PNPSIC model. As one important application, we present a numerical scheme for computing the electric current of a single ion species flowing over the selectivity filter, which we have implemented as a part of our PNPSIC software package. Moreover, we report a comparison of our predicted current–voltage curves (or I-V curves) with those generated from biophysical experiments [33,34] to further validate our PNPSIC model.

The rest of the paper is organized as follows. In Section 2, we present the PNPSIC model. In Section 3, we present a PNPSIC solution decomposition. In Section 4, we present the variational formulations of the boundary value problems

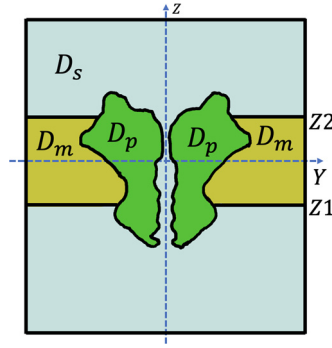


Fig. 1. An illustration of the protein, solvent, and membrane regions D_p , D_s , and D_m given in the box domain partition (1) and the membrane location numbers $Z1$ and $Z2$.

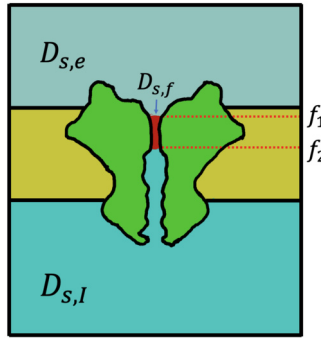


Fig. 2. An illustration of the filter $D_{s,f}$ (in red), intracellular and extracellular domains $D_{s,I}$ and $D_{s,e}$, and filter location numbers f_1 and f_2 given in the solvent region partition (2). (For interpretation of the colors in the figure(s), the reader is referred to the web version of this article.)

from the PNPSIC model and solution decomposition. In Section 5, we present the PNPSIC finite element approximation. In Section 6, we present the PNPSIC iterative method. In Section 7, we report our PNPSIC package and numerical results. In Section 8, we present an electric current computing scheme and validate computed I-V curves by biophysical experimental data. Finally, conclusions are made in Section 9.

2. Poisson-Nernst-Planck single ion channel model

Let a rectangular box open domain, Ω , be defined by

$$\Omega = \{(x, y, z) | L_{x_1} < x < L_{x_2}, L_{y_1} < y < L_{y_2}, L_{z_1} < z < L_{z_2}\},$$

such that it contains a membrane region, D_m , a solvent region, D_s , and a protein region, D_p , satisfying the partition

$$\Omega = D_p \cup D_m \cup D_s, \tag{1}$$

where L_{x_1} , L_{x_2} , L_{y_1} , L_{y_2} , L_{z_1} , and L_{z_2} are real numbers, D_p hosts a single ion channel protein, and D_s contains an ionic solution. Here we have set the origin of the rectangular coordinate system at the center of the ion channel protein and the z -axis direction to be one membrane normal direction. The membrane location can then be determined by the two numbers $Z1$ and $Z2$ of the z -axis. An illustration of the box domain partition (1) is given in Fig. 1.

Let $D_{s,f}$ denote the ion selectivity filter of a single ion channel protein. Since it only allows the ions of a single species to enter across the membrane, it separates the solvent domain D_s into an intracellular domain, $D_{s,I}$, and an extracellular domain, $D_{s,e}$, yielding the natural partition of D_s :

$$D_s = D_{s,f} \cup D_{s,I} \cup D_{s,e}. \tag{2}$$

With two selectivity filter location numbers, denoted by f_1 and f_2 , we can express the three solvent subdomains $D_{s,f}$, $D_{s,I}$, and $D_{s,e}$ as

$$D_{s,f} = \{\mathbf{r} \in D_s \mid \mathbf{r} = (x, y, z) \text{ with } f_1 \leq z \leq f_2\},$$

$$D_{s,I} = \{\mathbf{r} \in D_s \mid \mathbf{r} = (x, y, z) \text{ with } z < f_1\}, \quad D_{s,e} = \{\mathbf{r} \in D_s \mid \mathbf{r} = (x, y, z) \text{ with } z > f_2\}.$$

An illustration of the above solvent subdomains is given in Fig. 2.

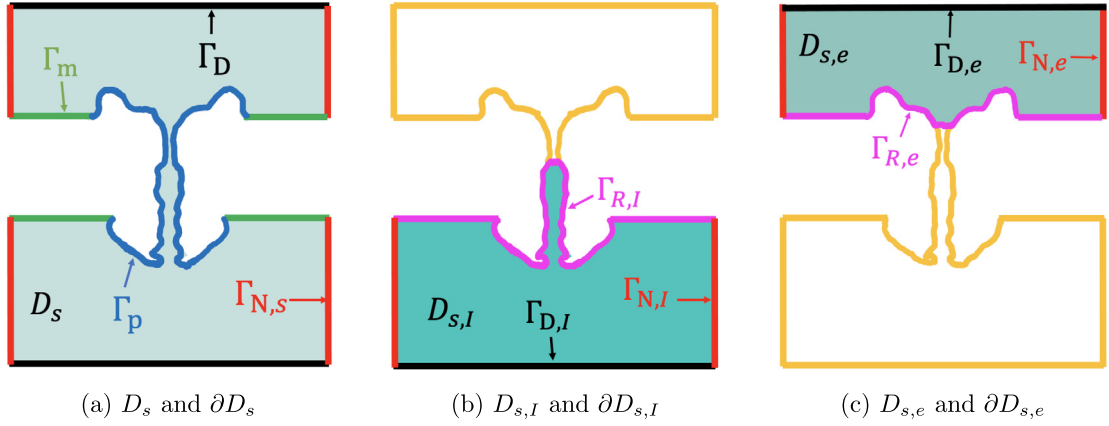


Fig. 3. An illustration of the solvent domain D_s , the intracellular and extracellular domains $D_{s,I}$ and $D_{s,e}$, and their boundary surface partitions given in (3).

The boundary of Ω consists of six surfaces. For clarity, we denote its bottom surface by $\Gamma_{D,I}$, top surface by $\Gamma_{D,e}$, the bottom and top surfaces by Γ_D , and the four side surfaces by Γ_N . We then express the boundaries ∂D_s , $\partial D_{s,I}$, and $\partial D_{s,e}$ of D_s , $D_{s,I}$, and $D_{s,e}$ as follows:

$$\partial D_s = \Gamma_D \cup \Gamma_{N,s} \cup \Gamma_m \cup \Gamma_p, \quad \partial D_{s,I} = \Gamma_{D,I} \cup \Gamma_{N,I} \cup \Gamma_{R,I}, \quad \partial D_{s,e} = \Gamma_{D,e} \cup \Gamma_{N,e} \cup \Gamma_{R,e}, \quad (3)$$

where $\Gamma_{N,s}$, $\Gamma_{N,I}$, and $\Gamma_{N,e}$ denote the side surfaces of D_s , $D_{s,I}$, and $D_{s,e}$, respectively; Γ_m denotes the interface between D_m and D_s ; Γ_p denotes the interface between D_p and D_s ; $\Gamma_{R,I}$ denotes the intracellular surface; and $\Gamma_{R,e}$ denotes the extracellular surface. An illustration of these boundary surfaces is given in Fig. 3.

We now construct the single ion channel model in the steady state. For clarity, we set Species 1 as the single ion species and denote its ionic concentration function by c_1 . Clearly, c_1 is defined in the solvent domain D_s since the ions of the single ion species are allowed to pass the selectivity filter across the membrane. We also define a dimensionless potential function, u , by

$$u(\mathbf{r}) = \frac{e_c}{k_B T} \Phi(\mathbf{r}), \quad \mathbf{r} \in \Omega, \quad (4)$$

where Φ is an electrostatic potential function in volts, e_c is the elementary charge, k_B is the Boltzmann constant, and T is the absolute temperature.

Following our previous work [2], we define c_1 by the Nernst-Planck boundary value problem:

$$\nabla \cdot \mathcal{D}_1(\mathbf{r}) [\nabla c_1(\mathbf{r}) + Z_1 c_1(\mathbf{r}) \nabla u(\mathbf{r})] = 0, \quad \mathbf{r} \in D_s, \quad (5a)$$

$$c_1(\mathbf{s}) = g_1(\mathbf{s}), \quad \mathbf{s} \in \Gamma_D, \quad (5b)$$

$$\frac{\partial c_1(\mathbf{s})}{\partial \mathbf{n}_s(\mathbf{s})} = 0, \quad \mathbf{s} \in \Gamma_{N,s}, \quad (5c)$$

$$\frac{\partial c_1(\mathbf{s})}{\partial \mathbf{n}_s(\mathbf{s})} + Z_1 c_1(\mathbf{s}) \frac{\partial u(\mathbf{s})}{\partial \mathbf{n}_s(\mathbf{s})} = 0, \quad \mathbf{s} \in \Gamma_p \cup \Gamma_m, \quad (5d)$$

where \mathcal{D}_1 and Z_1 are the diffusion function and charge number of Species 1, respectively, g_1 is a boundary value function, and \mathbf{n}_s denotes the unit outward normal direction of D_s .

Because of the selectivity filter $D_{s,f}$, the mixture solutions within the intracellular and extracellular domains $D_{s,I}$ and $D_{s,e}$ can be different. Thus, in general, $D_{s,I}$ can contain a mixture of n_I ionic species while $D_{s,e}$ contains another mixture of n_e ionic species so that we need two different sets of concentration functions, denoted by $\{c_{i,I}\}_{i=1}^{n_I}$ and $\{c_{i,e}\}_{i=1}^{n_e}$, to describe the ionic distributions within $D_{s,I}$ and $D_{s,e}$, respectively. Here n_I and n_e denote the numbers of ionic species within $D_{s,I}$ and $D_{s,e}$, respectively. Note that both $D_{s,I}$ and $D_{s,e}$ contain the ions of Species 1. Hence, we can set $c_{1,I} = c_1$ and $c_{1,e} = c_1$ for clarity. We then define the concentration functions $c_{i,I}$ for $i = 2, 3, \dots, n_I$ within $D_{s,I}$ using Nernst-Planck equations as follows:

$$\nabla \cdot \mathcal{D}_{i,I}(\mathbf{r}) [\nabla c_{i,I}(\mathbf{r}) + Z_{i,I} c_{i,I}(\mathbf{r}) \nabla u(\mathbf{r})] = 0, \quad \mathbf{r} \in D_{s,I}, \quad (6a)$$

$$c_{i,I}(\mathbf{s}) = g_{i,I}(\mathbf{s}), \quad \mathbf{s} \in \Gamma_{D,I}, \quad (6b)$$

$$\frac{\partial c_{i,I}(\mathbf{s})}{\partial \mathbf{n}_s(\mathbf{s})} = 0, \quad \mathbf{s} \in \Gamma_{N,I}, \quad (6c)$$

$$\frac{\partial c_{i,l}(\mathbf{s})}{\partial \mathbf{n}_s(\mathbf{s})} + Z_{i,l}c_{i,l}(\mathbf{s})\frac{\partial u(\mathbf{s})}{\partial \mathbf{n}_s(\mathbf{s})} = 0, \quad \mathbf{s} \in \Gamma_{R,l}, \tag{6d}$$

and $c_{i,e}$ for $i = 2, 3, \dots, n_e$ within $D_{s,e}$ by

$$\nabla \cdot \mathcal{D}_{i,e}(\mathbf{r}) [\nabla c_{i,e}(\mathbf{r}) + Z_{i,e}c_{i,e}(\mathbf{r})\nabla u(\mathbf{r})] = 0, \quad \mathbf{r} \in D_{s,e}, \tag{7a}$$

$$c_{i,e}(\mathbf{s}) = g_{i,e}(\mathbf{s}), \quad \mathbf{s} \in \Gamma_{D,e}, \tag{7b}$$

$$\frac{\partial c_{i,e}(\mathbf{s})}{\partial \mathbf{n}_s(\mathbf{s})} = 0, \quad \mathbf{s} \in \Gamma_{N,e}, \tag{7c}$$

$$\frac{\partial c_{i,e}(\mathbf{s})}{\partial \mathbf{n}_s(\mathbf{s})} + Z_{i,e}c_{i,e}(\mathbf{s})\frac{\partial u(\mathbf{s})}{\partial \mathbf{n}_s(\mathbf{s})} = 0, \quad \mathbf{s} \in \Gamma_{R,e}, \tag{7d}$$

where $\mathcal{D}_{i,l}$ and $\mathcal{D}_{i,e}$ are two diffusion functions; $g_{i,l}$ and $g_{i,e}$ are two boundary value functions; and $Z_{i,l}$ and $Z_{i,e}$ denote the charge numbers of Species i within $D_{s,l}$ and $D_{s,e}$, respectively.

Note that we have used the Neumann boundary value conditions (5c), (6c), and (7c) to reflect the fact that none of ions come from the side surfaces of the box domain. We also have used the Robin boundary value conditions (5d), (6d), and (7d) to reflect the fact that the membrane surfaces and ion channel walls are insulating (i.e., charged particles cannot penetrate them).

We next define the dimensionless potential function u in the box domain Ω .

We assume that a molecular structure of the single channel protein is given. Thus, a charge density function, ρ_p , within the protein region D_p can be estimated by

$$\rho_p = e_c \sum_{j=1}^{n_p} z_j \delta_{\mathbf{r}_j},$$

where n_p is the number of atoms, z_j and \mathbf{r}_j are the charge number and position vector of atom j , respectively, and $\delta_{\mathbf{r}_j}$ denotes the Dirac delta distribution at \mathbf{r}_j .

Using the concentration functions c_1 , $\{c_{i,l}\}_{i=2}^{n_l}$, and $\{c_{i,e}\}_{i=2}^{n_e}$ defined in (5), (6), and (7), we can estimate the charge density functions ρ_l , ρ_f , and ρ_e within the intracellular domain $D_{s,l}$, filter domain $D_{s,f}$, and extracellular domain $D_{s,e}$ by

$$\rho_l = e_c [Z_1 c_1(\mathbf{r}) + \sum_{i=2}^{n_l} Z_{i,l} c_{i,l}(\mathbf{r})], \quad \rho_f = e_c Z_1 c_1, \quad \rho_e = e_c [Z_1 c_1(\mathbf{r}) + \sum_{i=2}^{n_e} Z_{i,e} c_{i,e}(\mathbf{r})].$$

We then use Poisson equations to define u in D_p , D_m , $D_{s,l}$, $D_{s,f}$, and $D_{s,e}$, respectively, as follows:

$$-\epsilon_p \Delta u(\mathbf{r}) = \alpha \sum_{j=1}^{n_p} z_j \delta_{\mathbf{r}_j}, \quad \mathbf{r} \in D_p, \tag{8a}$$

$$-\epsilon_m \Delta u(\mathbf{r}) = 0, \quad \mathbf{r} \in D_m, \tag{8b}$$

$$-\epsilon_s \Delta u(\mathbf{r}) = \beta [Z_1 c_1(\mathbf{r}) + \sum_{i=2}^{n_l} Z_{i,l} c_{i,l}(\mathbf{r})], \quad \mathbf{r} \in D_{s,l}, \tag{8c}$$

$$-\epsilon_s \Delta u(\mathbf{r}) = \beta Z_1 c_1(\mathbf{r}), \quad \mathbf{r} \in D_{s,f}, \tag{8d}$$

$$-\epsilon_s \Delta u(\mathbf{r}) = \beta [Z_1 c_1(\mathbf{r}) + \sum_{i=2}^{n_e} Z_{i,e} c_{i,e}(\mathbf{r})], \quad \mathbf{r} \in D_{s,e}, \tag{8e}$$

where ϵ_p , ϵ_m , and ϵ_s are the permittivity constants within D_p , D_m , and D_s , respectively, and α and β denote the two model parameters to be given in (11). Note that none of charges from the membrane domain D_m are considered in (8b) and the permittivity constant ϵ_s is retained in the filter region $D_{s,f}$ as done commonly in PNP ion channel modeling.

Similarly to what are done in [2,3], we can obtain the following three interface conditions:

$$u(\mathbf{s}^-) = u(\mathbf{s}^+), \quad \epsilon_p \frac{\partial u(\mathbf{s}^-)}{\partial \mathbf{n}_p(\mathbf{s})} = \epsilon_s \frac{\partial u(\mathbf{s}^+)}{\partial \mathbf{n}_p(\mathbf{s})}, \quad \mathbf{s} \in \Gamma_p, \tag{9a}$$

$$u(\mathbf{s}^-) = u(\mathbf{s}^+), \quad \epsilon_m \frac{\partial u(\mathbf{s}^-)}{\partial \mathbf{n}_m(\mathbf{s})} = \epsilon_s \frac{\partial u(\mathbf{s}^+)}{\partial \mathbf{n}_m(\mathbf{s})} + \tau \sigma(\mathbf{s}), \quad \mathbf{s} \in \Gamma_m, \tag{9b}$$

$$u(\mathbf{s}^-) = u(\mathbf{s}^+), \quad \epsilon_p \frac{\partial u(\mathbf{s}^-)}{\partial \mathbf{n}_p(\mathbf{s})} = \epsilon_m \frac{\partial u(\mathbf{s}^+)}{\partial \mathbf{n}_p(\mathbf{s})}, \quad \mathbf{s} \in \Gamma_{pm}, \tag{9c}$$

and the following mixed boundary value conditions:

$$u(\mathbf{s}) = g(\mathbf{s}), \quad \mathbf{s} \in \Gamma_D \quad (\text{Dirichlet boundary condition}), \tag{10a}$$

$$\frac{\partial u(\mathbf{s})}{\partial \mathbf{n}_b(\mathbf{s})} = 0, \quad \mathbf{s} \in \Gamma_N \quad (\text{Neumann boundary condition}), \tag{10b}$$

where \mathbf{n}_p , \mathbf{n}_m , and \mathbf{n}_b are the unit outward normal directions of D_p , D_m , and Ω , respectively; Γ_{pm} denotes the interfaces between D_p and D_m ; g is a boundary value function; σ denotes a membrane surface charge density function; and τ is a related scaling constant as given in (11). Here σ is introduced for the purpose of partially reflecting the charge effects from the membrane domain.

A combination of (8) with (9) and (10) gives the boundary value interface problem for defining u in the box domain Ω . Consequently, we derive the **Poisson-Nernst-Planck single ion channel (PNPSIC) model** as a system of the boundary value interface problem in the box domain Ω and the three boundary value problems (5), (6), and (7) in the solvent domain D_s , intracellular domain $D_{s,I}$, and extracellular domain $D_{s,e}$. A solution of the PNPSIC model gives the potential function u and ionic concentrations c_1 , $\{c_{i,I}\}_{i=2}^{n_I}$, and $\{c_{i,e}\}_{i=2}^{n_e}$.

In the PNPSIC model, we use the following physical units: angstroms (Å) for length, moles per liter (mol/L) for ionic concentrations, volts for the potential function Φ , Kelvins (K) for temperature, Coulombs (C) for charges, squared angstroms per picosecond (Å²/ps) for diffusion functions, and micro-coulombs per squared centimeter ($\mu\text{C}/\text{cm}^2$) for the surface charge density σ . These units are often adopted to ion channel modelings and simulations. Under these units, we can derive the expressions of the model parameters α , β , and τ as follows:

$$\alpha = \frac{10^{10} e_c^2}{\epsilon_0 k_B T}, \quad \beta = \frac{N_A e_c^2}{10^{17} \epsilon_0 k_B T}, \quad \tau = \frac{10^{-12} e_c}{\epsilon_0 k_B T}, \tag{11}$$

where ϵ_0 is the permittivity of the vacuum and N_A is the Avogadro constant, which gives the number of ions per mole. With the values of ϵ_0 , e_c , k_B , and T listed in [35, Table 1] and $N_A = 6.02214129 \times 10^{23}$, we can estimate the values of α , β , and τ as

$$\alpha \approx 7042.9399, \quad \beta \approx 4.2414, \quad \tau \approx 4.392.$$

In numerical tests, we can set $\epsilon_p = 2$, $\epsilon_s = 80$, $\epsilon_m = 2$, and a value of σ between 0 and 30.

Similarly to what is done in [2], we define the membrane surface charge density σ and the boundary value functions g_1 and g by the piecewise expressions:

$$\sigma(\mathbf{s}) = \begin{cases} \sigma_I, & \mathbf{s} \in \Gamma_{m,I}, \\ \sigma_e, & \mathbf{s} \in \Gamma_{m,e}, \end{cases} \quad g_1(\mathbf{s}) = \begin{cases} g_{1,I}, & \mathbf{s} \in \Gamma_{D,I}, \\ g_{1,e}, & \mathbf{s} \in \Gamma_{D,e}, \end{cases} \quad g(\mathbf{s}) = \begin{cases} u_I, & \mathbf{s} \in \Gamma_{D,I}, \\ u_e, & \mathbf{s} \in \Gamma_{D,e}, \end{cases} \tag{12}$$

where σ_I and σ_e denote the surface charge density functions on the membrane intracellular and extracellular surfaces $\Gamma_{m,I}$ and $\Gamma_{m,e}$, respectively; $g_{1,I}$ and $g_{1,e}$ are two boundary value functions; u_I and u_e are two boundary potential functions.

When u is known, we recover the electrostatic potential function Φ by

$$\Phi(\mathbf{r}) = \frac{k_B T}{e_c} u(\mathbf{r}), \quad \mathbf{r} \in \Omega.$$

At $T = 298.5$ Kelvins, the factor $\frac{k_B T}{e_c}$ can be estimated as

$$\frac{k_B T}{e_c} \approx 0.026 \text{ volts.}$$

Thus, $u = 1$ corresponds to about 0.026 volts. Hence, from the boundary value functions u_I and u_e of (12) we can derive a voltage, V , across the membrane in volts by

$$V = \frac{k_B T}{e_c} (u_I - u_e) \approx 0.026 (u_I - u_e) \text{ volts.} \tag{13}$$

In practice, we often set $u_e = 0$ so that for a voltage in millivolts (mV), u_I can be estimated by

$$u_I = 10^{-3} \frac{e_c}{k_B T} V \approx 0.038921 V. \tag{14}$$

For example, to get a voltage of 100 mV, we can set $u_I = 3.8921$ and $u_e = 0$.

3. PNPSIC solution decomposition

To overcome the singularity difficulty caused by atomic charges, we can follow what is done in [2] to split the electrostatic potential function u as follows:

$$u(\mathbf{r}) = G(\mathbf{r}) + \Psi(\mathbf{r}) + \tilde{\Phi}(\mathbf{r}) \quad \forall \mathbf{r} \in \Omega, \tag{15}$$

where G is given by

$$G(\mathbf{r}) = \frac{\alpha}{4\pi\epsilon_p} \sum_{j=1}^{n_p} \frac{Z_j}{|\mathbf{r} - \mathbf{r}_j|}, \tag{16}$$

$\Psi(\mathbf{r})$ is a solution of a linear interface boundary value problem as follows:

$$\left\{ \begin{array}{ll} \Delta \Psi(\mathbf{r}) = 0, & \mathbf{r} \in D_p \cup D_s \cup D_m, \\ \Psi(\mathbf{s}^-) = \Psi(\mathbf{s}^+), \quad \epsilon_p \frac{\partial \Psi(\mathbf{s}^-)}{\partial \mathbf{n}_p(\mathbf{s})} = \epsilon_s \frac{\partial \Psi(\mathbf{s}^+)}{\partial \mathbf{n}_p(\mathbf{s})} + (\epsilon_s - \epsilon_p) \frac{\partial G(\mathbf{s})}{\partial \mathbf{n}_p(\mathbf{s})}, & \mathbf{s} \in \Gamma_p, \\ \Psi(\mathbf{s}^-) = \Psi(\mathbf{s}^+), \quad \epsilon_m \frac{\partial \Psi(\mathbf{s}^-)}{\partial \mathbf{n}_m(\mathbf{s})} = \epsilon_s \frac{\partial \Psi(\mathbf{s}^+)}{\partial \mathbf{n}_m(\mathbf{s})} + (\epsilon_s - \epsilon_m) \frac{\partial G(\mathbf{s})}{\partial \mathbf{n}_m(\mathbf{s})} + \tau \sigma(\mathbf{s}), & \mathbf{s} \in \Gamma_m, \\ \Psi(\mathbf{s}^-) = \Psi(\mathbf{s}^+), \quad \epsilon_p \frac{\partial \Psi(\mathbf{s}^-)}{\partial \mathbf{n}_p(\mathbf{s})} = \epsilon_m \frac{\partial \Psi(\mathbf{s}^+)}{\partial \mathbf{n}_p(\mathbf{s})} + (\epsilon_m - \epsilon_p) \frac{\partial G(\mathbf{s})}{\partial \mathbf{n}_p(\mathbf{s})}, & \mathbf{s} \in \Gamma_{pm}, \\ \frac{\partial \Psi(\mathbf{s})}{\partial \mathbf{n}_p(\mathbf{s})} = -\frac{\partial G(\mathbf{s})}{\partial \mathbf{n}_p(\mathbf{s})}, & \mathbf{s} \in \Gamma_N, \\ \Psi(\mathbf{s}) = g(\mathbf{s}) - G(\mathbf{s}), & \mathbf{s} \in \Gamma_D, \end{array} \right. \tag{17}$$

and $\tilde{\Phi}$ satisfies the linear interface boundary value problem:

$$\left\{ \begin{array}{ll} \Delta \tilde{\Phi}(\mathbf{r}) = 0, & \mathbf{r} \in D_m \cup D_p, \\ -\epsilon_s \Delta \tilde{\Phi}(\mathbf{r}) = \beta [Z_1 c_1(\mathbf{r}) + \sum_{i=2}^{n_l} Z_{i,l} c_{i,l}(\mathbf{r})], & \mathbf{r} \in D_{s,l}, \\ -\epsilon_s \Delta \tilde{\Phi}(\mathbf{r}) = \beta Z_1 c_1(\mathbf{r}), & \mathbf{r} \in D_{s,f}, \\ -\epsilon_s \Delta \tilde{\Phi}(\mathbf{r}) = \beta [Z_1 c_1(\mathbf{r}) + \sum_{i=2}^{n_e} Z_{i,e} c_{i,e}(\mathbf{r})], & \mathbf{r} \in D_{s,e}, \\ \tilde{\Phi}(\mathbf{s}^+) = \tilde{\Phi}(\mathbf{s}^-), \quad \epsilon_p \frac{\partial \tilde{\Phi}(\mathbf{s}^-)}{\partial \mathbf{n}_p(\mathbf{s})} = \epsilon_s \frac{\partial \tilde{\Phi}(\mathbf{s}^+)}{\partial \mathbf{n}_p(\mathbf{s})}, & \mathbf{s} \in \Gamma_p, \\ \tilde{\Phi}(\mathbf{s}^+) = \tilde{\Phi}(\mathbf{s}^-), \quad \epsilon_m \frac{\partial \tilde{\Phi}(\mathbf{s}^-)}{\partial \mathbf{n}_m(\mathbf{s})} = \epsilon_s \frac{\partial \tilde{\Phi}(\mathbf{s}^+)}{\partial \mathbf{n}_m(\mathbf{s})}, & \mathbf{s} \in \Gamma_m, \\ \tilde{\Phi}(\mathbf{s}^-) = \tilde{\Phi}(\mathbf{s}^+), \quad \epsilon_p \frac{\partial \tilde{\Phi}(\mathbf{s}^-)}{\partial \mathbf{n}_p(\mathbf{s})} = \epsilon_m \frac{\partial \tilde{\Phi}(\mathbf{s}^+)}{\partial \mathbf{n}_p(\mathbf{s})}, & \mathbf{s} \in \Gamma_{pm}, \\ \frac{\partial \tilde{\Phi}(\mathbf{s})}{\partial \mathbf{n}_p(\mathbf{s})} = 0, & \mathbf{s} \in \Gamma_N, \\ \tilde{\Phi}(\mathbf{s}) = 0, & \mathbf{s} \in \Gamma_D. \end{array} \right. \tag{18}$$

Here, $\frac{\partial G(\mathbf{s})}{\partial \mathbf{n}(\mathbf{s})} = \nabla G(\mathbf{s}) \cdot \mathbf{n}(\mathbf{s})$, and ∇G can be found in the expression

$$\nabla G(\mathbf{s}) = -\frac{\alpha}{4\pi\epsilon_p} \sum_{j=1}^{n_p} Z_j \frac{(\mathbf{s} - \mathbf{r}_j)}{|\mathbf{s} - \mathbf{r}_j|^3}.$$

Note that the boundary value problem (18) only depends on ionic concentrations. Hence, we can treat G , Ψ , and their gradient vectors $\nabla G(\mathbf{r})$ and $\nabla \Psi(\mathbf{r})$ as known functions during a search for $\tilde{\Phi}$ and ionic concentrations. Thus, we introduce a function, w , by

$$w(\mathbf{r}) = G(\mathbf{r}) + \Psi(\mathbf{r}), \quad \mathbf{r} \in \Omega, \tag{19}$$

and treat it as a known function. We then substitute the potential function u with $\tilde{\Phi} + w$ to modify the boundary value problems (5), (6), and (7) as follows:

- The boundary value problem (5) is modified as

$$\left\{ \begin{array}{ll} \nabla \cdot \mathcal{D}_1(\mathbf{r}) \left[\nabla c_1(\mathbf{r}) + Z_1 c_1(\mathbf{r}) \nabla (\tilde{\Phi}(\mathbf{r}) + w(\mathbf{r})) \right] = 0, & \mathbf{r} \in D_s, \\ c_1(\mathbf{s}) = g_1(\mathbf{s}), & \mathbf{s} \in \Gamma_{D,l} \cup \Gamma_{D,e}, \\ \frac{\partial c_1(\mathbf{s})}{\partial \mathbf{n}_s(\mathbf{s})} = 0, & \mathbf{s} \in \Gamma_{N,s}, \\ \frac{\partial c_1(\mathbf{s})}{\partial \mathbf{n}_s(\mathbf{s})} + Z_1 c_1(\mathbf{s}) \frac{\partial (\tilde{\Phi}(\mathbf{s}) + w(\mathbf{s}))}{\partial \mathbf{n}_s(\mathbf{s})} = 0, & \mathbf{s} \in \Gamma_p \cup \Gamma_m. \end{array} \right. \tag{20}$$

- The boundary value problem (6) is modified as

$$\begin{cases} \nabla \cdot \mathcal{D}_{i,l}(\mathbf{r}) \left[\nabla c_{i,l}(\mathbf{r}) + Z_{i,l} c_{i,l}(\mathbf{r}) \nabla(\tilde{\Phi}(\mathbf{r}) + w(\mathbf{r})) \right] = 0, & \mathbf{r} \in D_{s,l}, \\ c_{i,l}(\mathbf{s}) = g_{i,l}(\mathbf{s}), & \mathbf{s} \in \Gamma_{D,l}, \\ \frac{\partial c_{i,l}(\mathbf{s})}{\partial \mathbf{n}_s(\mathbf{s})} = 0, & \mathbf{s} \in \Gamma_{N,l}, \\ \frac{\partial c_{i,l}(\mathbf{s})}{\partial \mathbf{n}_s(\mathbf{s})} + Z_{i,l} c_{i,l}(\mathbf{s}) \frac{\partial(\tilde{\Phi} + w)}{\partial \mathbf{n}_s(\mathbf{s})} = 0, & \mathbf{s} \in \Gamma_{R,l}. \end{cases} \tag{21}$$

- The boundary value problem (7) is modified as

$$\begin{cases} \nabla \cdot \mathcal{D}_{i,e}(\mathbf{r}) \left[\nabla c_{i,e}(\mathbf{r}) + Z_{i,e} c_{i,e}(\mathbf{r}) \nabla(\tilde{\Phi}(\mathbf{r}) + w(\mathbf{r})) \right] = 0, & \mathbf{r} \in D_{s,e}, \\ c_{i,e}(\mathbf{s}) = g_{i,e}(\mathbf{s}), & \mathbf{s} \in \Gamma_{D,e}, \\ \frac{\partial c_{i,e}(\mathbf{s})}{\partial \mathbf{n}_s(\mathbf{s})} = 0, & \mathbf{s} \in \Gamma_{N,e}, \\ \frac{\partial c_{i,e}(\mathbf{s})}{\partial \mathbf{n}_s(\mathbf{s})} + Z_{i,e} c_{i,e}(\mathbf{s}) \frac{\partial(\tilde{\Phi}(\mathbf{s}) + w(\mathbf{s}))}{\partial \mathbf{n}_s(\mathbf{s})} = 0, & \mathbf{s} \in \Gamma_{R,e}. \end{cases} \tag{22}$$

A combination of the above modified boundary value problems with (18) gives a nonlinear system for computing $\tilde{\Phi}$, c_1 , $\{c_{i,l}\}_{i=2}^{n_l}$, and $\{c_{i,e}\}_{i=2}^{n_e}$. Similarly to what is done in [2,35], we can show that this system is well defined without involving any singularity point of u . Hence, this system can be much easier to solve numerically than the original PNPSIC model. Since the linear boundary value interface problem (17) has been solved numerically in our previous work [2], we focus on the numerical solution of this nonlinear system in this paper.

4. Variational formulations

One key step for us to develop a PNPSIC finite element solver is to reformulate the boundary value problems (17), (18), (20), (21), and (22) into variational forms. To do so, we introduce the following function spaces

$$V(\Omega) = \{u \in H^1(\Omega) \mid u = 0 \text{ on } \Gamma_D\}, \quad V(D_s) = \{v \in H^1(D_s) \mid v = 0 \text{ on } \Gamma_D\}, \tag{23}$$

$$V(D_{s,l}) = \{v \in H^1(D_{s,l}) \mid v = 0 \text{ on } \Gamma_{D,l}\}, \quad V(D_{s,e}) = \{v \in H^1(D_{s,e}) \mid v = 0 \text{ on } \Gamma_{D,e}\}, \tag{24}$$

where $H^1(\Omega)$, $H^1(D_s)$, $H^1(D_{s,l})$, and $H^1(D_{s,e})$ denote the regular Sobolev function spaces defined in the box domain Ω and solvent domains D_s , $D_{s,l}$, and $D_{s,e}$, respectively [36]. We then define a bilinear functional, $a(u, v)$, for $u \in H^1(\Omega)$ and $v \in V(\Omega)$ by

$$a(u, v) = \epsilon_p \int_{D_p} \nabla u \cdot \nabla v \, d\mathbf{r} + \epsilon_m \int_{D_m} \nabla u \cdot \nabla v \, d\mathbf{r} + \epsilon_s \int_{D_s} \nabla u \cdot \nabla v \, d\mathbf{r}. \tag{25}$$

Following what was done in our previous work [2], we can obtain the variational problems of the boundary value problems (17), (18), (20), (21), and (22) as follows:

- 1. Variational problem of (17):** Find $\Psi \in H^1(\Omega)$ satisfying $\Psi = g - G$ on Γ_D such that

$$\begin{aligned} a(\Psi, v) = & (\epsilon_s - \epsilon_p) \int_{\Gamma_p} \frac{\partial G(\mathbf{s})}{\partial \mathbf{n}_p(\mathbf{s})} v \, ds + (\epsilon_s - \epsilon_m) \int_{\Gamma_m} \frac{\partial G(\mathbf{s})}{\partial \mathbf{n}_m(\mathbf{s})} v \, ds + (\epsilon_m - \epsilon_p) \int_{\Gamma_{pm}} \frac{\partial G(\mathbf{s})}{\partial \mathbf{n}_p(\mathbf{s})} v \, ds \\ & - \epsilon_m \int_{\Gamma_N \cap \partial D_m} \frac{\partial G(\mathbf{s})}{\partial \mathbf{n}_b(\mathbf{s})} v \, ds - \epsilon_s \int_{\Gamma_{N,s}} \frac{\partial G(\mathbf{s})}{\partial \mathbf{n}_b(\mathbf{s})} v \, ds + \tau \int_{\Gamma_m} \sigma v \, ds \quad \forall v \in V(\Omega), \end{aligned} \tag{26}$$

where ∂D_m denotes the boundary of membrane domain D_m and $\Gamma_{N,s} = \Gamma_N \cap \partial D_s$.

- 2. Variational problem of (18):** Find $\tilde{\Phi} \in V(\Omega)$ such that

$$\begin{aligned} a(\tilde{\Phi}, v) = & \beta \int_{D_{s,l}} \left[Z_{1,l} c_1(\mathbf{r}) + \sum_{j=2}^{n_l} Z_{j,l} c_{j,l}(\mathbf{r}) \right] v(\mathbf{r}) \, d\mathbf{r} + \beta \int_{D_{s,f}} Z_{1,l} c_1(\mathbf{r}) v(\mathbf{r}) \, d\mathbf{r} \\ & + \beta \int_{D_{s,e}} \left[Z_{1,e} c_1(\mathbf{r}) + \sum_{j=2}^{n_e} Z_{j,e} c_{j,e}(\mathbf{r}) \right] v(\mathbf{r}) \, d\mathbf{r} \quad \forall v \in V(\Omega). \end{aligned} \tag{27}$$

3. Variational problem of (20): Find $c_1 \in H^1(D_s)$ satisfying $c_1 = g_1$ on Γ_D such that

$$\int_{D_s} \mathcal{D}_1 \left[\nabla c_1(\mathbf{r}) + Z_1 c_1(\mathbf{r}) \nabla(\tilde{\Phi}(\mathbf{r}) + w(\mathbf{r})) \right] \nabla v(\mathbf{r}) d\mathbf{r} = 0 \quad \forall v \in V(D_s), \tag{28}$$

subject to the sign constraint conditions $c_1 > 0$.

4. Variational problem of (21): Find $c_{i,l} \in H^1(D_{s,l})$ satisfying $c_{i,l} = g_{i,l}$ on $\Gamma_{D,l}$ such that

$$\int_{D_{s,l}} \mathcal{D}_{i,l} \left[\nabla c_{i,l}(\mathbf{r}) + Z_{i,l} c_{i,l}(\mathbf{r}) \nabla(\tilde{\Phi}(\mathbf{r}) + w(\mathbf{r})) \right] \nabla v d\mathbf{r} = 0 \quad \forall v \in V(D_{s,l}), \tag{29}$$

subject to the sign constraint conditions $c_{i,l} > 0$ for $i = 2, 3, \dots, n$.

5. Variational problem of (22): Find $c_{i,e} \in H^1(D_{s,e})$ satisfying $c_{i,e} = g_{i,e}$ on $\Gamma_{D,e}$ such that

$$\int_{D_{s,e}} \mathcal{D}_{i,e} \left[\nabla c_{i,e}(\mathbf{r}) + Z_{i,e} c_{i,e}(\mathbf{r}) \nabla(\tilde{\Phi}(\mathbf{r}) + w(\mathbf{r})) \right] \nabla v d\mathbf{r} = 0 \quad \forall v \in V(D_{s,e}), \tag{30}$$

subject to the sign constraint conditions $c_{i,e} > 0$ for $i = 2, 3, \dots, n$.

Here w is defined in (19) and has been calculated prior to solving (28), (29), and (30).

However, the sign constraint conditions may cause difficulties in the numerical solutions of the variational problems (28), (29), and (30). To overcome such difficulties, we introduce the Slotboom variable transformations

$$c_1 = e^{-Z_1 u} \bar{c}_1, \quad c_{i,l} = e^{-Z_{i,l} u} \bar{c}_{i,l}, \quad c_{i,e} = e^{-Z_{i,e} u} \bar{c}_{i,e}, \tag{31}$$

where \bar{c}_1 , $\bar{c}_{i,l}$, and $\bar{c}_{i,e}$ are called the Slotboom variables.

With (31), we can get the identities

$$\begin{aligned} \nabla c_1 + Z_1 c_1 \nabla u &= e^{-Z_1 u} \nabla \bar{c}_1, \\ \nabla c_{i,l} + Z_{i,l} c_{i,l} \nabla u &= e^{-Z_{i,l} u} \nabla \bar{c}_{i,l}, \\ \nabla c_{i,e} + Z_{i,e} c_{i,e} \nabla u &= e^{-Z_{i,e} u} \nabla \bar{c}_{i,e}. \end{aligned} \tag{32}$$

Using the boundary conditions (5c), (5d), (6c), (6d), (7c), (7d), and (10), and the fact that $e^{-Z_{i,l} u} > 0$ and $e^{-Z_{i,e} u} > 0$, we can obtain the Neumann boundary conditions

$$\begin{aligned} \frac{\partial \bar{c}_1(\mathbf{s})}{\partial \mathbf{n}_b(\mathbf{s})} &= 0, \quad \mathbf{s} \in \Gamma_{N,s}, & \frac{\partial \bar{c}_1(\mathbf{s})}{\partial \mathbf{n}_s(\mathbf{s})} &= 0, \quad \mathbf{s} \in \Gamma_p \cup \Gamma_m, \\ \frac{\partial \bar{c}_{i,l}(\mathbf{s})}{\partial \mathbf{n}_b(\mathbf{s})} &= 0, \quad \mathbf{s} \in \Gamma_{N,l}, & \frac{\partial \bar{c}_{i,l}(\mathbf{s})}{\partial \mathbf{n}_s(\mathbf{s})} &= 0, \quad \mathbf{s} \in \Gamma_{R,l}, \\ \frac{\partial \bar{c}_{i,e}(\mathbf{s})}{\partial \mathbf{n}_b(\mathbf{s})} &= 0, \quad \mathbf{s} \in \Gamma_{N,e}, & \frac{\partial \bar{c}_{i,e}(\mathbf{s})}{\partial \mathbf{n}_s(\mathbf{s})} &= 0, \quad \mathbf{s} \in \Gamma_{R,e}, \end{aligned}$$

and the Dirichlet boundary conditions

$$\bar{c}_1(\mathbf{s}) = \bar{g}_1(\mathbf{s}) \text{ on } \Gamma_D, \quad \bar{c}_{i,l}(\mathbf{s}) = \bar{g}_{i,l}(\mathbf{s}) \text{ on } \Gamma_{D,l}, \quad \bar{c}_{i,e}(\mathbf{s}) = \bar{g}_{i,e}(\mathbf{s}) \text{ on } \Gamma_{D,e},$$

where $\bar{g}_1 = e^{Z_1} g_1$, $\bar{g}_{i,l} = e^{Z_{i,l}} g_{i,l}$, and $\bar{g}_{i,e} = e^{Z_{i,e}} g_{i,e}$.

Applying (32) and the above boundary value conditions to (28), (29), and (30), we can derive the variational problems that define the Slotboom variables \bar{c}_1 , $\bar{c}_{i,l}$, and $\bar{c}_{i,e}$ as follows:

1. Variational problem for defining \bar{c}_1 : Find $\bar{c}_1 \in H^1(D_s)$ with $\bar{c}_1 = \bar{g}_1$ on Γ_D such that

$$\int_{D_s} \mathcal{D}_1 e^{-Z_1(\tilde{\Phi}+w)} \nabla \bar{c}_1 \nabla v d\mathbf{r} = 0 \quad \forall v \in V(D_s). \tag{33}$$

2. Variational problem for defining $\bar{c}_{i,l}$: Find $\bar{c}_{i,l} \in H^1(D_{s,l})$ with $\bar{c}_{i,l} = \bar{g}_{i,l}$ on $\Gamma_{D,l}$ for $i = 2, 3, \dots, n_l$ such that

$$\int_{D_{s,l}} \mathcal{D}_{i,l} e^{-Z_{i,l}(\tilde{\Phi}+w)} \nabla \bar{c}_{i,l} \nabla v_i d\mathbf{r} = 0 \quad \forall v_i \in V(D_{s,l}) \text{ for } i = 2, 3, \dots, n_l. \tag{34}$$

3. Variational problem for defining $\bar{c}_{i,e}$: Find $\bar{c}_{i,e} \in H^1(D_{s,e})$ with $\bar{c}_{i,e} = \bar{g}_{i,e}$ on $\Gamma_{D,e}$ for $i = 2, 3, \dots, n_e$ such that

$$\int_{D_{s,e}} \mathcal{D}_{i,e} e^{-Z_{i,e}(\tilde{\Phi}+w)} \nabla \bar{c}_{i,e} \nabla v_i d\mathbf{r} = 0 \quad \forall v_i \in V(D_{s,e}) \text{ for } i = 2, 3, \dots, n_e. \tag{35}$$

Note that the boundary value problems (33), (34), and (35) do not involve any sign constraint condition since their solutions \bar{c}_1 , $\bar{c}_{i,l}$, and $\bar{c}_{i,e}$ are always positive (see [37, page 27] for a proof).

Furthermore, we use (31) to transform the variational equation (27) to a nonlinear variational problem as follows: Find $\tilde{\Phi} \in V(\Omega)$ such that

$$a(\tilde{\Phi}, v) - b(\tilde{\Phi}, \bar{c}_1, \bar{c}_{2,l}, \bar{c}_{3,l}, \dots, \bar{c}_{n_l,l}, \bar{c}_{2,e}, \bar{c}_{3,e}, \dots, \bar{c}_{n_e,e}; v) = 0 \quad \forall v \in V(\Omega), \tag{36}$$

where the bilinear functional $a(\cdot, \cdot)$ is defined in (25) and the nonlinear functional b is defined by

$$b(\tilde{\Phi}, \bar{c}_1, \bar{c}_{2,l}, \bar{c}_{3,l}, \dots, \bar{c}_{n_l,l}, \bar{c}_{2,e}, \bar{c}_{3,e}, \dots, \bar{c}_{n_e,e}; v) = \beta \int_{D_{s,l}} v(\mathbf{r}) \sum_{j=2}^{n_l} Z_{j,l} e^{-Z_{j,l}(\tilde{\Phi}+w)} \bar{c}_{j,l}(\mathbf{r}) d\mathbf{r} \\ + \beta \int_{D_s} Z_1 e^{-Z_1(\tilde{\Phi}+w)} \bar{c}_1(\mathbf{r}) v(\mathbf{r}) d\mathbf{r} + \beta \int_{D_{s,e}} v(\mathbf{r}) \sum_{j=2}^{n_e} Z_{j,e} e^{-Z_{j,e}(\tilde{\Phi}+w)} \bar{c}_{j,e}(\mathbf{r}) d\mathbf{r}. \tag{37}$$

We now combine (36) with (33), (34), and (35) to derive a system of nonlinear variational equations for computing the functions $\tilde{\Phi}$, \bar{c}_1 , $\{\bar{c}_{j,l}\}_{j=2}^{n_l}$, and $\{\bar{c}_{j,e}\}_{j=2}^{n_e}$ as follows:

Find $\tilde{\Phi} \in V(\Omega)$, $\bar{c}_1 \in H^1(D_s)$ with $\bar{c}_1 = \bar{g}_1$ on Γ_D , $\bar{c}_{i,l} \in H^1(D_{s,l})$ with $\bar{c}_{i,l} = \bar{g}_{i,l}$ on $\Gamma_{D,l}$ for $i = 2, 3, \dots, n_l$, and $\bar{c}_{i,e} \in H^1(D_{s,e})$ with $\bar{c}_{i,e} = \bar{g}_{i,e}$ on $\Gamma_{D,e}$ for $i = 2, 3, \dots, n_e$ such that

$$\begin{cases} \int_{D_s} \mathcal{D}_1 e^{-Z_1(\tilde{\Phi}+w)} \nabla \bar{c}_1 \nabla v d\mathbf{r} = 0 \quad \forall v \in V(D_s), \\ \int_{D_{s,l}} \mathcal{D}_{i,l} e^{-Z_{i,l}(\tilde{\Phi}+w)} \nabla \bar{c}_{i,l} \nabla v_i d\mathbf{r} = 0 \quad \forall v_i \in V(D_{s,l}) \text{ for } i = 2, 3, \dots, n_l, \\ \int_{D_{s,e}} \mathcal{D}_{i,e} e^{-Z_{i,e}(\tilde{\Phi}+w)} \nabla \bar{c}_{i,e} \nabla v_i d\mathbf{r} = 0 \quad \forall v_i \in V(D_{s,e}) \text{ for } i = 2, 3, \dots, n_e, \\ a(\tilde{\Phi}, v) - b(\tilde{\Phi}, \bar{c}_1, \bar{c}_{2,l}, \bar{c}_{3,l}, \dots, \bar{c}_{n_l,l}, \bar{c}_{2,e}, \bar{c}_{3,e}, \dots, \bar{c}_{n_e,e}; v) = 0 \quad \forall v \in V(\Omega), \end{cases} \tag{38}$$

where $w = G + \Psi$ with G and Ψ being given in (16) and (26), respectively, which have been calculated prior to solving the above system.

When a solution of the nonlinear system (38) is found, we can use (31) to derive the ionic concentration functions c_1 , $\{c_{i,l}\}_{i=2}^{n_l}$, and $\{c_{i,e}\}_{i=2}^{n_e}$, and claim them to be positive due to the positivity of the Slotboom variable functions \bar{c}_1 , $\{\bar{c}_{i,l}\}_{i=2}^{n_l}$, and $\{\bar{c}_{i,e}\}_{i=2}^{n_e}$. Furthermore, we use (15) to derive the potential function u . Consequently, we obtain a solution of the PNPSIC model.

5. A finite element approximation

In this section, we present a finite element approximation to the nonlinear variational system (38). We start with a generation of a tetrahedral mesh, $D_{p,h}$, of the protein region D_p , a tetrahedral mesh, $D_{m,h}$, of the membrane region D_m , and a tetrahedral mesh, $D_{s,h}$, of the solvent region D_s . Using them, we construct an interface fitted tetrahedral mesh, Ω_h , of the box domain Ω by

$$\Omega_h = D_{p,h} \cup D_{m,h} \cup D_{s,h}.$$

We then from the solvent mesh $D_{s,h}$ extract a tetrahedral mesh, $D_{s,l,h}$, of the intracellular domain $D_{s,l}$, a tetrahedral mesh, $D_{s,f,h}$, of the selectivity filter domain $D_{s,f}$, and a tetrahedral mesh, $D_{s,e,h}$, of the extracellular domain $D_{s,e}$ such that they satisfy

$$D_{s,l,h} \cup D_{s,f,h} \cup D_{s,e,h} = D_{s,h}.$$

Using these meshes, we construct four linear Lagrange finite element spaces, denoted by $\mathcal{U}(\Omega_h)$, $\mathcal{U}(D_{s,h})$, $\mathcal{U}(D_{s,l,h})$, and $\mathcal{U}(D_{s,e,h})$, as the finite dimensional subspaces of the function spaces $H^1(\Omega)$, $H^1(D_s)$, $H^1(D_{s,l})$, and $H^1(D_{s,e})$, respectively. We then define their subspaces $\mathcal{V}(\Omega_h)$, $\mathcal{V}(D_{s,h})$, $\mathcal{V}(D_{s,l,h})$, and $\mathcal{V}(D_{s,e,h})$ by

$$\mathcal{V}(\Omega_h) = \{u \in \mathcal{U}(\Omega_h) \mid u = 0 \text{ on } \Gamma_D\}, \quad \mathcal{V}(D_{s,h}) = \{v \in \mathcal{U}(D_{s,h}) \mid v = 0 \text{ on } \Gamma_D\}, \\ \mathcal{V}(D_{s,l,h}) = \{v \in \mathcal{U}(D_{s,l,h}) \mid v = 0 \text{ on } \Gamma_{D,l}\}, \quad \mathcal{V}(D_{s,e,h}) = \{v \in \mathcal{U}(D_{s,e,h}) \mid v = 0 \text{ on } \Gamma_{D,e}\}.$$

To communicate functions from one finite element function space to another one, we construct three restriction operators,

$$\mathcal{R}_s : \mathcal{U}(\Omega_h) \rightarrow \mathcal{U}(D_{s,h}), \quad \mathcal{R}_l : \mathcal{U}(\Omega_h) \rightarrow \mathcal{U}(D_{s,l,h}), \quad \mathcal{R}_e : \mathcal{U}(\Omega_h) \rightarrow \mathcal{U}(D_{s,e,h}), \tag{39}$$

as the natural restrictions. That is, for any $u \in \mathcal{U}(\Omega_h)$,

$$\mathcal{R}_s u(\mathbf{r}) = u(\mathbf{r}) \text{ for } \mathbf{r} \in D_{s,h}, \mathcal{R}_l u(\mathbf{r}) = u(\mathbf{r}) \text{ for } \mathbf{r} \in D_{s,l,h}, \text{ and } \mathcal{R}_e u(\mathbf{r}) = u(\mathbf{r}) \text{ for } \mathbf{r} \in D_{s,e,h}, \tag{40}$$

since the meshes $D_{s,h}$, $D_{s,l,h}$, and $D_{s,e,h}$ are the submeshes of the box mesh Ω_h .

We also construct three prolongation operators,

$$\mathcal{P}_s : \mathcal{U}(D_{s,h}) \rightarrow \mathcal{U}(\Omega_h), \quad \mathcal{P}_l : \mathcal{U}(D_{s,l,h}) \rightarrow \mathcal{U}(\Omega_h), \quad \mathcal{P}_e : \mathcal{U}(D_{s,e,h}) \rightarrow \mathcal{U}(\Omega_h). \tag{41}$$

as the natural extensions in the following senses:

$$\mathcal{P}_s u(\mathbf{r}) = \begin{cases} u(\mathbf{r}), & \mathbf{r} \in D_{s,h}, \\ 0, & \text{otherwise} \end{cases} \text{ for } u \in \mathcal{U}(D_{s,h}), \tag{42}$$

$$\mathcal{P}_l u(\mathbf{r}) = \begin{cases} u(\mathbf{r}), & \mathbf{r} \in D_{s,l,h}, \\ 0, & \text{otherwise} \end{cases} \text{ for } u \in \mathcal{U}(D_{s,l,h}), \tag{43}$$

$$\mathcal{P}_e u(\mathbf{r}) = \begin{cases} u(\mathbf{r}), & \mathbf{r} \in D_{s,e,h}, \\ 0, & \text{otherwise} \end{cases} \text{ for } u \in \mathcal{U}(D_{s,e,h}). \tag{44}$$

Using the above finite element spaces and operators, we can derive a finite element approximation of (38) as a system of nonlinear finite element equations as follows:

Find $\tilde{\Phi} \in \mathcal{V}(\Omega_h)$, $\bar{c}_1 \in \mathcal{U}(D_{s,h})$ with $\bar{c}_1 = \bar{g}_1$ on Γ_D , $\bar{c}_{i,l} \in \mathcal{U}(D_{s,l,h})$ with $\bar{c}_{i,l} = \bar{g}_{i,l}$ on $\Gamma_{D,l}$ for $i = 2, 3, \dots, n_l$, and $\bar{c}_{i,e} \in \mathcal{U}(D_{s,e,h})$ with $\bar{c}_{i,e} = \bar{g}_{i,e}$ for $i = 2, 3, \dots, n_e$ on $\Gamma_{D,e}$ such that

$$\begin{cases} \int_{D_{s,h}} \mathcal{D}_1 e^{-Z_1 \mathcal{R}_s(\tilde{\Phi}+w)} \nabla \bar{c}_1 \nabla v \, d\mathbf{r} = 0 & \forall v \in \mathcal{V}(D_{s,h}), \\ \int_{D_{s,l,h}} \mathcal{D}_{i,l} e^{-Z_{i,l} \mathcal{R}_l(\tilde{\Phi}+w)} \nabla \bar{c}_{i,l} \nabla v_i \, d\mathbf{r} = 0 & \forall v_i \in \mathcal{V}(D_{s,l,h}), \quad i = 2, 3, \dots, n_l, \\ \int_{D_{s,e,h}} \mathcal{D}_{i,e} e^{-Z_{i,e} \mathcal{R}_e(\tilde{\Phi}+w)} \nabla \bar{c}_{i,e} \nabla v_i \, d\mathbf{r} = 0 & \forall v_i \in \mathcal{V}(D_{s,e,h}), \quad i = 2, 3, \dots, n_e, \\ a_h(\tilde{\Phi}, v) - b_h(\tilde{\Phi}, \bar{c}_1, \bar{c}_{2,l}, \bar{c}_{3,l}, \dots, \bar{c}_{n_l,l}, \bar{c}_{2,e}, \bar{c}_{3,e}, \dots, \bar{c}_{n_e,e}; v) = 0 & \forall v \in \mathcal{V}(\Omega_h), \end{cases} \tag{45}$$

where $w = G + \Psi$ with Ψ being calculated as a finite element solution of the linear variational problem (26) with $\Psi \in \mathcal{U}(\Omega_h)$ and $v \in \mathcal{V}(\Omega_h)$, $a_h(\tilde{\Phi}, v)$ is defined by

$$a_h(\tilde{\Phi}, v) = \epsilon_p \int_{D_{p,h}} \nabla \tilde{\Phi} \cdot \nabla v \, d\mathbf{r} + \epsilon_m \int_{D_{m,h}} \nabla \tilde{\Phi} \cdot \nabla v \, d\mathbf{r} + \epsilon_s \int_{D_{s,h}} \nabla \tilde{\Phi} \cdot \nabla v \, d\mathbf{r}, \tag{46}$$

which is a finite element approximation of (25), and b_h is defined by

$$\begin{aligned} b_h(\tilde{\Phi}, \bar{c}_1, \bar{c}_{2,l}, \bar{c}_{3,l}, \dots, \bar{c}_{n_l,l}, \bar{c}_{2,e}, \bar{c}_{3,e}, \dots, \bar{c}_{n_e,e}; v) &= \beta Z_1 \int_{D_{s,h}} e^{-Z_1(\tilde{\Phi}+w)} \mathcal{P}_s \bar{c}_1(\mathbf{r}) v(\mathbf{r}) \, d\mathbf{r} \\ &+ \beta \int_{D_{s,l,h}} v(\mathbf{r}) \sum_{j=2}^{n_l} Z_{j,l} e^{-Z_{j,l}(\tilde{\Phi}+w)} \mathcal{P}_l \bar{c}_{j,l}(\mathbf{r}) \, d\mathbf{r} + \beta \int_{D_{s,e,h}} v(\mathbf{r}) \sum_{j=2}^{n_e} Z_{j,e} e^{-Z_{j,e}(\tilde{\Phi}+w)} \mathcal{P}_e \bar{c}_{j,e}(\mathbf{r}) \, d\mathbf{r}. \end{aligned} \tag{47}$$

which is a finite element approximation of (37).

6. Nonlinear finite element iterative methods

In this section, we present a block relaxation iterative scheme for solving the nonlinear system (45), along with a modified Newton iterative method for solving each related nonlinear finite element equation. Let $\tilde{\Phi}^k, \bar{c}_1^k, \{\bar{c}_{i,l}^k\}_{i=2}^{n_l}$, and $\{\bar{c}_{i,e}^k\}_{i=2}^{n_e}$ denote the k th iterates generated from the block relaxation iterative scheme. When the initial iterates $\tilde{\Phi}^0, \bar{c}_1^0, \{\bar{c}_{i,l}^0\}_{i=2}^{n_l}$, and $\{\bar{c}_{i,e}^0\}_{i=2}^{n_e}$ are given, we define the $(k + 1)$ th iterates $\tilde{\Phi}^{k+1}, \bar{c}_1^{k+1}, \{\bar{c}_{i,l}^{k+1}\}_{i=2}^{n_l}$, and $\{\bar{c}_{i,e}^{k+1}\}_{i=2}^{n_e}$ for $k \geq 0$ as follows:

$$\bar{c}_1^{k+1} = \bar{c}_1^k + \omega(\bar{p}_1 - \bar{c}_1^k), \tag{48a}$$

$$\bar{c}_{i,l}^{k+1} = \bar{c}_{i,l}^k + \omega(\bar{p}_{i,l} - \bar{c}_{i,l}^k), \quad i = 2, 3, \dots, n_l, \tag{48b}$$

$$\bar{c}_{i,e}^{k+1} = \bar{c}_{i,e}^k + \omega(\bar{p}_{i,e} - \bar{c}_{i,e}^k), \quad i = 2, 3, \dots, n_e, \tag{48c}$$

$$\tilde{\Phi}^{k+1} = \tilde{\Phi}^k + \omega(\bar{q} - \tilde{\Phi}^k), \tag{48d}$$

where ω is a relaxation parameter between 0 and 2, \bar{p}_1 is a solution of the linear finite element problem: Find $\bar{p}_1 \in \mathcal{U}(D_{s,h})$ satisfying $\bar{p}_1 = \bar{g}_1$ on Γ_D such that

$$\int_{D_{s,h}} \mathcal{D}_1 e^{-Z_1 \mathcal{R}_s(\tilde{\Phi}^k+w)} \nabla \bar{p}_1 \nabla v \, d\mathbf{r} = 0 \quad \forall v \in \mathcal{V}(D_{s,h}), \tag{49}$$

$\bar{p}_{i,l}$ is a solution of the linear finite element problem: Find $\bar{p}_{i,l} \in \mathcal{U}(D_{s,l,h})$ satisfying $\bar{p}_{i,l} = \bar{g}_{i,l}$ on $\Gamma_{D,l}$ such that

$$\int_{D_{s,l,h}} \mathcal{D}_{i,l} e^{-Z_{i,l} \mathcal{R}_l(\tilde{\Phi}^k+w)} \nabla \bar{p}_{i,l} \nabla v_i \, d\mathbf{r} = 0 \quad \forall v_i \in \mathcal{V}(D_{s,l,h}), \quad i = 2, 3, \dots, n_l, \tag{50}$$

$\bar{p}_{i,e}$ is a solution of the linear finite element problem: Find $\bar{p}_{i,e} \in \mathcal{U}(D_{s,e,h})$ satisfying $\bar{p}_{i,e} = \bar{g}_{i,e}$ on $\Gamma_{D,e}$ such that

$$\int_{D_{s,e,h}} \mathcal{D}_{i,e} e^{-Z_{i,e} \mathcal{R}_e(\tilde{\Phi}^k+w)} \nabla \bar{p}_{i,e} \nabla v_i \, d\mathbf{r} = 0 \quad \forall v_i \in \mathcal{V}(D_{s,e,h}), \quad i = 2, 3, \dots, n_e, \tag{51}$$

and \bar{q} is a solution of the nonlinear finite element problem: Find $\bar{q} \in \mathcal{V}(\Omega_h)$ such that

$$a_h(\bar{q}, v) - b_h(\bar{q}, \bar{c}_1^{k+1}, \bar{c}_{2,l}^{k+1}, \bar{c}_{3,l}^{k+1}, \dots, \bar{c}_{n_l,l}^{k+1}, \bar{c}_{2,e}^{k+1}, \bar{c}_{3,e}^{k+1}, \dots, \bar{c}_{n_e,e}^{k+1}; v) = 0 \quad \forall v \in \mathcal{V}(\Omega_h), \tag{52}$$

where a_h and b_h are defined in (46) and (47), respectively, and $w = G + \Psi$, which has been calculated prior to the above iterations.

One simple selection of initial concentration iterates is to set

$$\bar{c}_1^0 = c_1^b, \quad \bar{c}_{i,l}^0 = c_{i,l}^b \text{ for } i = 2, 3, \dots, n_l, \quad \bar{c}_{i,e}^0 = c_{i,e}^b \text{ for } i = 2, 3, \dots, n_e,$$

where c_1^b is a bulk concentration of Species 1, $c_{i,l}^b$ is a bulk concentration of Species i in $D_{s,l}$, and $c_{i,e}^b$ is a bulk concentration of Species i in $D_{s,e}$. With such selections, the last equation of the nonlinear system (45) is reduced to a nonlinear equation of $\tilde{\Phi}$ as follows: Find $\tilde{\Phi} \in \mathcal{V}(\Omega_h)$ such that

$$\begin{aligned} a_h(\tilde{\Phi}, v) - \beta Z_1 c_1^b \int_{D_{s,h}} e^{-Z_1(\tilde{\Phi}+w)} v \, d\mathbf{r} - \beta \int_{D_{s,l,h}} v \sum_{j=2}^{n_l} Z_{j,l} c_{i,l}^b e^{-Z_{j,l}(\tilde{\Phi}+w)} \, d\mathbf{r} \\ - \beta \int_{D_{s,e,h}} v \sum_{j=2}^{n_e} Z_{j,e} c_{i,e}^b e^{-Z_{j,e}(\tilde{\Phi}+w)} \, d\mathbf{r} = 0 \quad \forall v \in \mathcal{V}(\Omega_h), \end{aligned} \tag{53}$$

Solving the above equation numerically gives the initial iterate $\tilde{\Phi}^0$.

We next present two modified Newton iterative methods for solving the nonlinear finite element systems (52) and (53), respectively.

Similar to what is done in [2], for each $k \geq 0$, we solve (52) by a modified Newton iterative method as defined below:

$$\bar{q}_k^{j+1} = \bar{q}_k^j + \xi_k^j, \quad j = 0, 1, 2, \dots,$$

where ξ_k^j is a solution of the linear variational problem: Find $\xi_k^j \in \mathcal{V}(\Omega_h)$ such that for all $v \in \mathcal{V}(\Omega_h)$,

$$\begin{aligned} a_h(\xi_k^j, v) + \beta Z_1^2 \int_{D_{s,h}} \mathcal{P}_s \bar{c}_1^{k+1} e^{-Z_1(\bar{q}_k^j+w)} \xi_k^j v \, d\mathbf{r} + \beta \int_{D_{s,l,h}} v \xi_k^j \sum_{i=2}^{n_l} Z_{i,l}^2 \mathcal{P}_l \bar{c}_{i,l}^{k+1} e^{-Z_{i,l}(\bar{q}_k^j+w)} \, d\mathbf{r} \\ + \beta \int_{D_{s,e,h}} v \xi_k^j \sum_{i=2}^{n_e} Z_{i,e}^2 \mathcal{P}_e \bar{c}_{i,e}^{k+1} e^{-Z_{i,e}(\bar{q}_k^j+w)} \, d\mathbf{r} = \beta \int_{D_{s,l,h}} v \sum_{i=2}^{n_l} Z_{i,l} \mathcal{P}_l \bar{c}_{i,l}^{k+1} e^{-Z_{i,l}(\bar{q}_k^j+w)} \, d\mathbf{r} \\ + \beta \int_{D_{s,e,h}} v \sum_{i=2}^{n_e} Z_{i,e} \mathcal{P}_e \bar{c}_{i,e}^{k+1} e^{-Z_{i,e}(\bar{q}_k^j+w)} \, d\mathbf{r} + \beta Z_1 \int_{D_{s,h}} \mathcal{P}_s \bar{c}_1^{k+1} e^{-Z_1(\bar{q}_k^j+w)} v \, d\mathbf{r} - a_h(\bar{q}_k^j, v), \end{aligned} \tag{54}$$

and \bar{q}_k^0 is an initial guess, which is set as $\tilde{\Phi}^{(0)}$ for $k = 0$ and $\tilde{\Phi}^k$ for $k \geq 1$, and a_h is defined in (46).

We also define a modified Newton iterative scheme for solving (53) by the recursive formula

$$\tilde{\Phi}^{(j+1)} = \tilde{\Phi}^{(j)} + \xi^j \quad \text{for } j = 0, 1, 2, \dots, \tag{55}$$

where $\tilde{\Phi}^{(j)}$ denotes the j th iterate of the modified Newton iterative scheme, ξ^j is a solution of the linear variational problem: Find $\xi^j \in \mathcal{V}(\Omega_h)$ such that

$$\begin{aligned}
& a(\xi^j, v) + \beta Z_1^2 c_1^b \int_{D_{s,h}} e^{-Z_1(\tilde{\Phi}^{(j)}+w)} \xi^j v d\mathbf{r} + \beta \int_{D_{s,l,h}} v \xi^j \sum_{i=2}^{n_l} Z_{i,l}^2 c_{i,l}^b e^{-Z_{i,l}(\tilde{\Phi}^{(j)}+w)} d\mathbf{r} \\
& + \beta \int_{D_{s,e,h}} v \xi^j \sum_{i=2}^{n_e} Z_{i,e}^2 c_{i,e}^b e^{-Z_{i,e}(\tilde{\Phi}^{(j)}+w)} d\mathbf{r} = \beta \int_{D_{s,l,h}} \sum_{i=2}^{n_l} Z_{i,l} c_{i,l}^b e^{-Z_{i,l}(\tilde{\Phi}^{(j)}+w)} d\mathbf{r} \\
& + \beta \int_{D_{s,e,h}} v \sum_{i=2}^{n_e} Z_{i,e} c_{i,e}^b e^{-Z_{i,e}(\tilde{\Phi}^{(j)}+w)} d\mathbf{r} + \beta Z_1 c_1^b \int_{D_{s,h}} e^{-Z_1(\tilde{\Phi}^{(j)}+w)} v d\mathbf{r} - a(\tilde{\Phi}^{(j)}, v) \quad \forall v \in \mathcal{V}(\Omega_h),
\end{aligned} \tag{56}$$

and $\tilde{\Phi}^{(0)}$ is a solution of a linearized problem of (53) as follows: Find $\tilde{\Phi}^{(0)} \in \mathcal{V}(\Omega_h)$ such that

$$\begin{aligned}
& a(\tilde{\Phi}^{(0)}, v) + \beta \sum_{i=2}^{n_l} Z_{i,l}^2 c_{i,l}^b \int_{D_{s,l,h}} v \tilde{\Phi}^{(0)} d\mathbf{r} + \beta \sum_{i=2}^{n_e} Z_{i,e}^2 c_{i,e}^b \int_{D_{s,e,h}} v \tilde{\Phi}^{(0)} d\mathbf{r} \\
& + \beta Z_1^2 c_1^b \int_{D_{s,h}} \tilde{\Phi}^{(0)} v d\mathbf{r} = -\beta Z_1^2 c_1^b \int_{D_{s,h}} w v d\mathbf{r} - \beta \sum_{i=2}^{n_l} Z_{i,l}^2 c_{i,l}^b \int_{D_{s,l,h}} w v d\mathbf{r} \\
& - \beta \sum_{i=2}^{n_e} Z_{i,e}^2 c_{i,e}^b \int_{D_{s,e,h}} w v d\mathbf{r} \quad \forall v \in \mathcal{V}(\Omega_h).
\end{aligned} \tag{57}$$

In the above linear variational problem, we have used the electroneutrality conditions:

$$Z_1 c_1^b + \sum_{i=2}^{n_l} Z_{i,l} c_{i,l}^b = 0 \text{ in } D_{s,l}, \quad Z_1 c_1^b + \sum_{i=2}^{n_e} Z_{i,e} c_{i,e}^b = 0 \text{ in } D_{s,e}.$$

In the above nonlinear iterations, we solve all the related linear finite element equations (49), (50), (51), (54), (56), and (57), numerically, by using either an iterative method such as the generalized minimal residual method using incomplete LU preconditioning (GMRES-ILU) or a direct method such as the LU factorization method.

We control the iterative process using the following termination rules:

$$\|\tilde{\Phi}^{k+1} - \tilde{\Phi}^k\| < \epsilon, \quad \|\bar{c}_1^{k+1} - \bar{c}_1^k\| < \epsilon, \quad \max_{2 \leq i \leq n_l} \|\bar{c}_{i,l}^{k+1} - \bar{c}_{i,l}^k\| < \epsilon, \quad \max_{2 \leq i \leq n_e} \|\bar{c}_{i,e}^{k+1} - \bar{c}_{i,e}^k\| < \epsilon, \tag{58}$$

where ϵ is a tolerance and $\|\cdot\|$ denotes the L_2 norm. By default, we set $\epsilon = 10^{-3}$.

7. Finite element package and numerical results

We developed a PNPSIC finite element program package in Python and Fortran based on the state-of-the-art finite element library from the FEniCS project [38], our PNP ion channel finite element software [2], and a new version of our ion channel finite element mesh program package [4], which we plan to report in another paper due to the length of its description. In fact, the implementation of our PNPSIC finite element solver requires three new tetrahedral meshes – an intracellular domain mesh, $D_{s,l,h}$, an extracellular domain mesh, $D_{s,e,h}$, and a selectivity filter mesh, $D_{s,f,h}$, which cannot be generated from our current mesh package; new mesh generation schemes are required to generate these new meshes. We did so and used them to update the current mesh package. We then adapted the updated mesh package as a part of our PNPSIC finite element program package.

To demonstrate the performance of the PNPSIC package, we did numerical tests for a potassium channel protein, called KcsA, since its potassium selectivity properties have been well studied (see [18] for example) and its molecular structure (with the protein data bank identification number (PDB ID) 1BL8) can be downloaded from the Orientations of Proteins in Membranes database <https://opm.phar.umich.edu>, along with the membrane location numbers $Z1 = -17$ and $Z2 = 17$. An illustration of the KcsA molecular structure is given in Plot (a) of Fig. 4, where we plotted the molecular structure in cartoon and three potassium ions in red balls to highlight the location of a narrow selectivity filter. From this figure it can be seen that there is an empty space below the filter, which is the location of an ionic solvent-filled cavity.

Using the molecular structure, we determined the selectivity filter location numbers $f_1 = 2$ and $f_2 = 14$ and generated a molecular triangular surface mesh of the KcsA channel by the MSMS software package (<https://ccsb.scripps.edu/msms/>). Here the two MSMS parameters were set as 0.6 for the triangulation mesh density and 1.0 for the radius of the probe ball to ensure the molecular surface to retain an open selectivity pore properly. We refined the triangular surface mesh to make it suitable for finite element calculation before generating tetrahedral meshes.

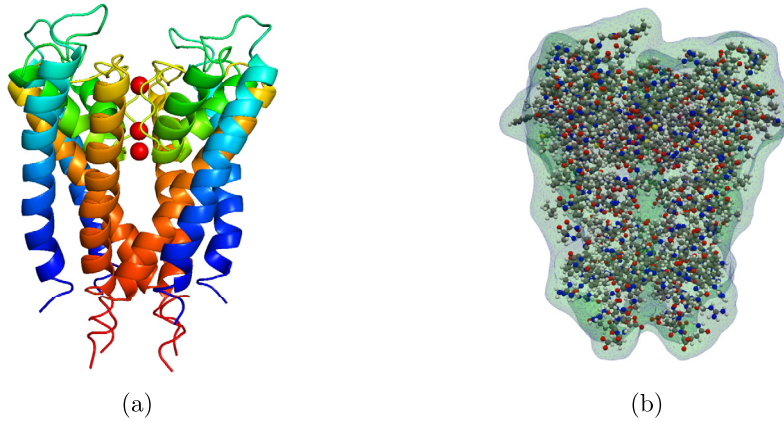


Fig. 4. (a) A molecular structure of the potassium channel protein (PDB ID: 1BL8) in cartoon with three potassium ions bound in the channel filter part (shown in red). (b) A view of the molecular structure in ball-stick warped by a protein tetrahedral mesh, $D_{p,h}$, generated by our mesh generation package. Here different atoms are represented as colored balls.

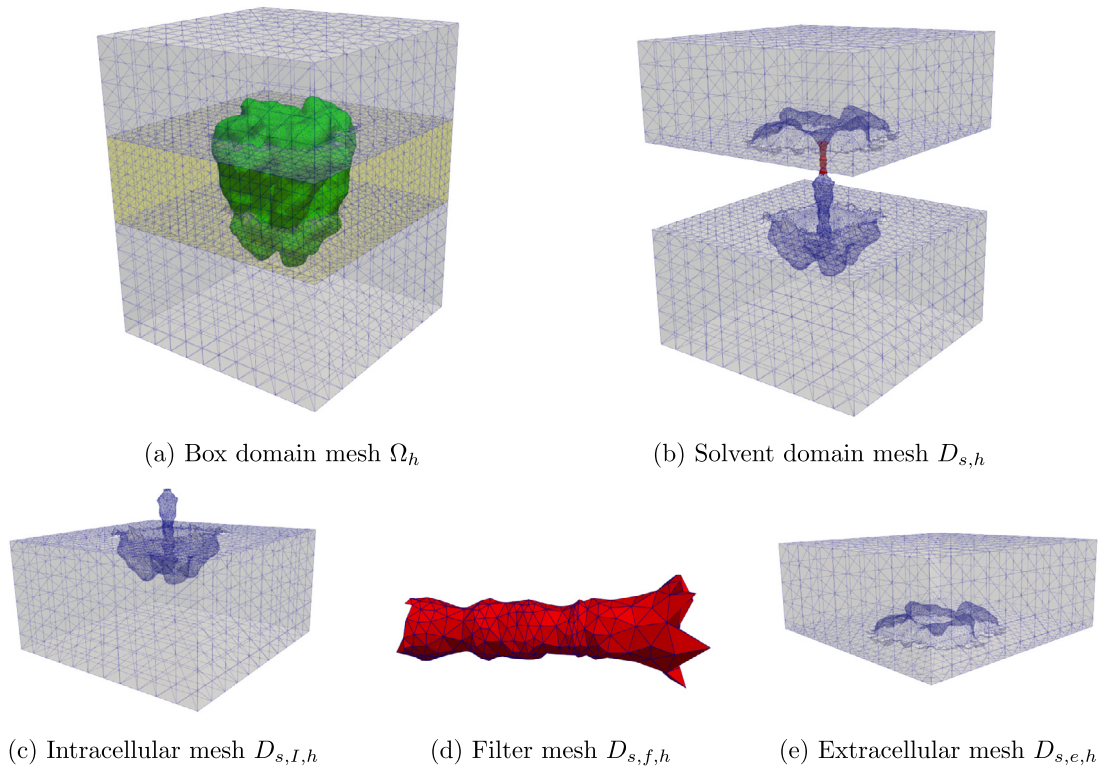


Fig. 5. Tetrahedral meshes generated by our mesh package for a potassium channel protein (PDB ID: 1BL8). In (a), the meshes of protein and membrane regions D_p and D_m are colored in green and yellow, respectively. In (b, d), the filter mesh $D_{s,f,h}$ is colored in red.

We set the box domain $\Omega = [-47, 47] \times [-47, 47] \times [-65, 54]$ and then generated an interface fitted tetrahedral box domain mesh, Ω_h , and the tetrahedral meshes $D_{s,l,h}$, $D_{s,e,h}$, $D_{s,f,h}$, and $D_{s,h}$ from our mesh generation package. The mesh data are listed in Table 1 and a view of these meshes is displayed in Fig. 5. To clearly display the complex interfaces Γ_p , Γ_m , and Γ_{pm} , we highlight the protein and membrane meshes in green and yellow colors, respectively, in Fig. 5(a). A comparison of the protein mesh domain $D_{p,h}$ with a van der Waals protein domain (a union of all atomic spheres of a molecule with each atom being treated as a sphere with a van der Waals atomic radius) is given in Fig. 4(b) to show that the mesh $D_{p,h}$ has high-quality in wrapping the geometric shape of the KcsA molecular structure. From Fig. 5 it can be seen that our tetrahedral meshes $D_{s,h}$, $D_{s,l,h}$, $D_{s,f,h}$, and $D_{s,e,h}$ have well retained the irregular geometric shapes of the solvent domains D_s , $D_{s,l}$, $D_{s,f}$, and $D_{s,e}$ and the complex interfaces of box domain Ω .

Table 1
Mesh data for the seven meshes used in numerical tests.

Number of Vertices						
Ω_h	$D_{p,h}$	$D_{s,h}$	$D_{m,h}$	$D_{s,l,h}$	$D_{s,e,h}$	$D_{s,f,h}$
33,024	25,077	12,822	11,454	7194	5305	306
Number of Tetrahedra						
198,805	111,847	47,450	39,508	26,370	20,087	798

Table 2
Convergence and performance of our nonlinear finite element iterative scheme (48) for solving the nonlinear system (45). Here lte denotes the number of iterations determined by the termination rule (58) and CPU the computer time spent by our PNPSIC package in seconds.

	$\omega = 0.8$		$\omega = 0.9$		$\omega = 1.0$		$\omega = 1.1$	
	lte	CPU	lte	CPU	lte	CPU	lte	CPU
Test 1	10	100.39	8	83.40	3	48.87	9	83.94
Test 2	11	102.16	8	81.68	7	61.78	13	93.06

In numerical tests, we used a mixture of 0.2 mol/L KCl and 0.1 mol/L NaCl within $D_{s,l}$ and $D_{s,e}$ and ordered the three ionic species K^+ , Na^+ , and Cl^- from 1 to 3 (i.e. $n_l = n_e = 3$). Thus, c_1 denotes the concentration of K^+ ions in D_s , $c_{2,l}$ the concentration of Na^+ ions in $D_{s,l}$, $c_{3,l}$ the concentration of Cl^- ions in $D_{s,l}$, $c_{2,e}$ the concentration of Na^+ ions in $D_{s,e}$, and $c_{3,e}$ the concentration of Cl^- ions in $D_{s,e}$. Also, the charge numbers and bulk concentrations of K^+ , Na^+ , and Cl^- are given by

$$Z_1 = 1, Z_{2,l} = Z_{2,e} = 1, Z_{3,l} = Z_{3,e} = -1, c_1^b = 0.2, c_{2,l}^b = c_{2,e}^b = 0.1, c_{3,l}^b = c_{3,e}^b = 0.3.$$

From the website <https://www.aqion.de/site/194> we got the diffusion constants D_1^b, D_2^b , and D_3^b for $K^+, Na^+,$ and Cl^- , respectively, as

$$D_1^b = 0.196, D_2^b = 0.133, D_3^b = 0.203.$$

Using them, we set the diffusion functions

$$D_{2,l}(\mathbf{r}) = D_2^b, D_{3,l}(\mathbf{r}) = D_3^b \quad \text{for } \mathbf{r} \in D_{s,l}, \quad D_{2,e}(\mathbf{r}) = D_2^b, \quad D_{3,e}(\mathbf{r}) = D_3^b \quad \text{for } \mathbf{r} \in D_{s,e}.$$

We also used a smooth diffusion function, D_1 , given in the expression

$$D_1(\mathbf{r}) = \begin{cases} D_1^b, & \mathbf{r} \in D_{s,l} \cup D_{s,e}, \\ D_1^f + (D_1^f - D_1^b)\mathcal{I}_t(\mathbf{r}), & \mathbf{r} \in D_{s,f} \text{ with } f_2 - \eta \leq z \leq f_2 \text{ (extracellular buffer)}, \\ D_1^f, & \mathbf{r} \in D_{s,f} \text{ with } f_1 + \eta \leq z \leq f_2 - \eta, \\ D_1^f + (D_1^f - D_1^b)\mathcal{I}_b(\mathbf{r}), & \mathbf{r} \in D_{s,f} \text{ with } f_1 \leq z \leq f_1 + \eta \text{ (intracellular buffer)}, \end{cases} \quad (59)$$

where D_1^f denotes a parameter for controlling a diffusion-limited conduction (or current) rate within the selectivity filter $D_{s,f}$ under a voltage across the membrane; \mathcal{I}_b and \mathcal{I}_t are the two interpolation functions given in [39, eq. (27)]; and η is a parameter for adjusting the size of a buffer region. Since none of the experimental values of D_1^f can be found in the literature, we can determine a proper value of D_1^f through fitting I-V experimental data in numerical tests.

For simplicity, we fixed the parameters $\eta = 3, \epsilon_p = 2, \epsilon_m = 2,$ and $\epsilon_s = 80$ in all the numerical tests. We then set $D_1^f = 0.01078$ and used the membrane surface charge density σ and boundary value functions g_1 and g given in (12) with $g_{i,l} = g_{i,e} = c_i^b$ and the following values of $u_l, u_e, \sigma_l,$ and σ_e in two particular tests, called Tests 1 and 2:

- Test 1.** A test using $u_l = 0, u_e = 0, \sigma_l = 0,$ and $\sigma_e = 0.$
- Test 2.** A test using $u_l = -1, u_e = 1, \sigma_l = -10,$ and $\sigma_e = 10.$

Note that in Test 1, we did not consider any external voltage and any membrane charge as a comparison to Test 2. We solved each related linear finite element equation, approximately, by a generalized minimal residual method using incomplete LU preconditioning with the absolute and relative residual error tolerances being 10^{-5} . The numerical tests were done on one core of our Mac Studio with Apple silicon M1 Max and 64 GB memory. Numerical results are reported in Tables 2 and 3 and Figs. 6 and 7.

Table 2 reports the number of iterations and computer CPU time produced by our nonlinear finite element iterative scheme (48) in the numerical solution of the nonlinear system (45). From it we can see that our scheme reached the smallest

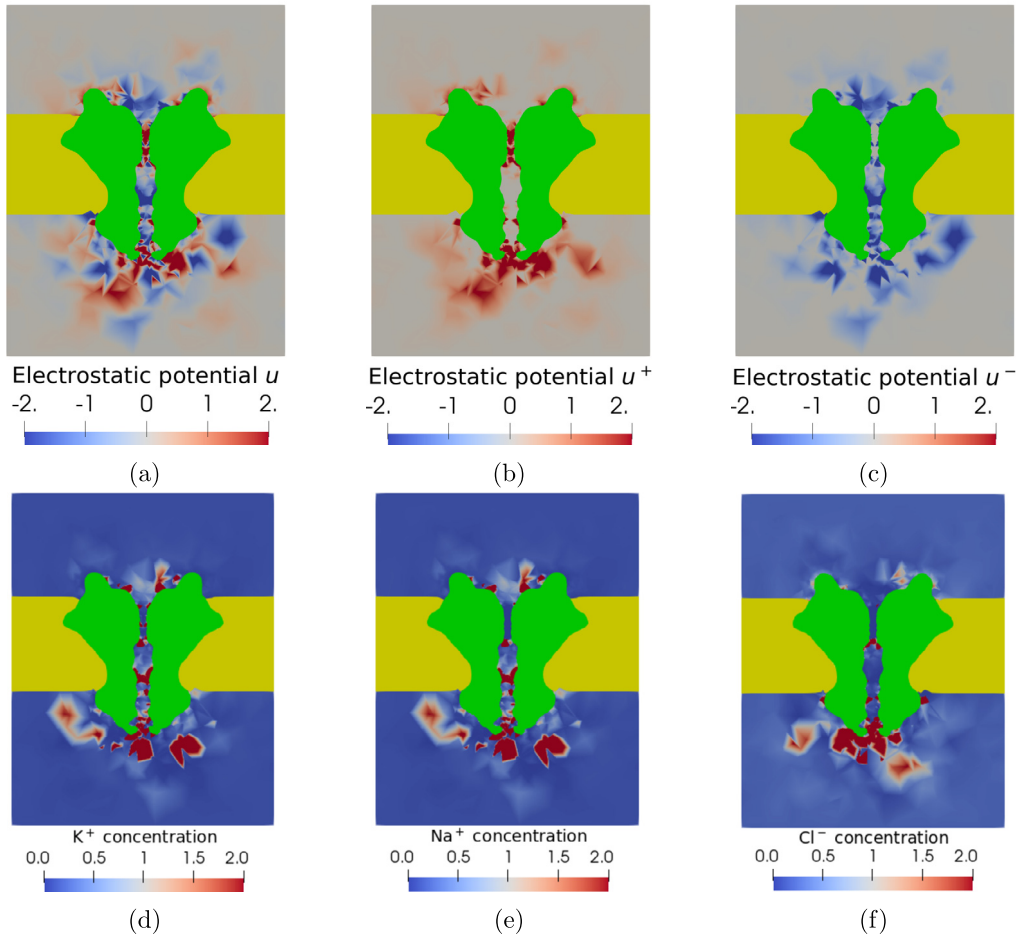


Fig. 6. A color mapping of the electrostatic potentials and ionic concentrations generated by our PNPSIC model in Test 1. Here the protein and membrane regions are colored in green and yellow, respectively, to clearly display the color mapping.

Table 3

Computer CPU time distributions for our PNPSIC package in seconds. Here $\omega = 1.0$ and \bar{c} denotes a set of $\bar{c}_1, \bar{c}_{2,I}, \bar{c}_{3,I}, \bar{c}_{2,e}$, and $\bar{c}_{3,e}$ defined in the nonlinear system (45).

	Compute $G, \nabla G$	Solve (26) for Ψ	Solve (53) for $\tilde{\Phi}^0$	Solve (45) for $\tilde{\Phi}$ and \bar{c}
Test 1	0.689	0.367	15.79	48.87
Test 2	0.686	0.371	16.16	61.78

number of iterations at $\omega = 1.0$ with three iterations in Test 1 and seven iterations in Test 2 to satisfy the termination rule (58), showing a fast rate of convergence. Note that our scheme in Test 2 took more iterations than in Test 1, indicating that the non-homogeneous boundary value conditions and membrane surface charges can cause the nonlinear system (45) to become more difficult to solve numerically.

Table 3 reports the CPU times spent on the four major parts of our PNPSIC software package for Tests 1 and 2 in seconds. From it we can see that the linear boundary value problem (26) was solved in only about 0.4 seconds by the GMRES using the ILU preconditioning. This indicates that the GMRES method is an effective linear iterative solver for our PNPSIC software package. Our modified Newton iterative method (55) took only about 16 seconds to solve the nonlinear finite element equation (53) for an initial guess, $\tilde{\Phi}^0$, demonstrating its efficiency in CPU time. Our iterative scheme (48) found a numerical solution of the nonlinear system (45) in about one minute only, showing the high computer performance of its program package.

Fig. 6 displays the color mappings of the electrostatic potentials u , u^+ , and u^- and the concentrations of cations K^+ and Na^+ and anions Cl^- on the cross section $x = 0$ of the solvent domain D_s in the case of Test 1. Here u^+ and u^- denote the positive and negative potential parts of u , whose sum gives u . We calculate them by

$$u^+(\mathbf{r}) = \frac{u(\mathbf{r}) + |u(\mathbf{r})|}{2}, \quad u^-(\mathbf{r}) = \frac{u(\mathbf{r}) - |u(\mathbf{r})|}{2}, \quad \mathbf{r} \in D_s. \tag{60}$$

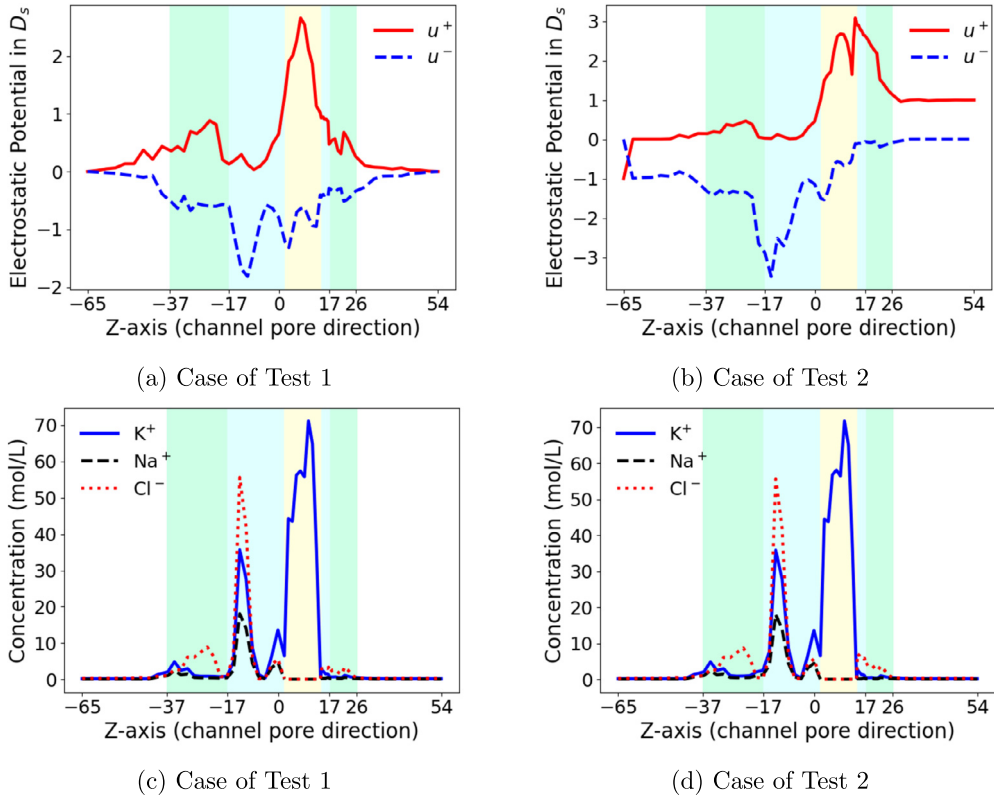


Fig. 7. The electrostatic potential functions u^+ and u^- and concentration functions of K^+ , Na^+ , and Cl^- produced by the PNPSIC model in Tests 1 and 2.

From Plot (c) it can be seen that the values of u^- , in blue color, are distributed mostly within the channel pore and surround the ion channel protein, attracting most K^+ and Na^+ ions as shown in Plots (d, e). From Plots (e, f) we do not see any sodium ion or any chloride ion within the selectivity filter, confirming that our PNPSIC model retains the potassium selectivity property.

In the area having negative electrostatic potential values, both potassium and sodium ions are found to have similar distribution patterns as shown in Plot (d, e), however, from which it is difficult for us to tell which species dominates the other since the color mapping only reflects the potential and concentration values on one across section. We need more color mappings to view more values. Doing so is prolix. Hence, we turn to using a 2D curve mapping scheme reported in [2] to explore their distribution profiles over the whole solvent domain D_s as done in Figs. 7 and 8.

In details, each point of a 2D curve in Figs. 7 and 8 represents an average value of a 3D function over a block of the solvent domain D_s . For example, the j -th point (z^j, c_1^j) of a 2D curve that represents a concentration function, c_1 , is set with z^j being the j -th partition number of the interval $[L_{z_1}, L_{z_2}]$ and c_1^j being an average value of c_1 over the j -th block B_j of a block partition of the solvent domain D_s , which is calculated by

$$c_1^j = \frac{1}{\|B_j\|} \int_{B_j} c_1(\mathbf{r}) d\mathbf{r}, \quad j = 1, 2, \dots, m,$$

where $\|B_j\|$ denotes the volume of B_j and m is the total number of blocks. In Figs. 7 and 8, we set $m = 70$, each block to have the same length 8 in the z -axis direction, and the set of partition numbers, $\{z^j\}_{j=1}^m$, to contain the membrane location numbers $Z1 = -17$ and $Z2 = 17$, the filter location numbers $f_1 = 2$ and $f_2 = 14$, and the channel pore location numbers, which we found as $z = -37$ and $z = 26$. We highlighted the filter interval $2 \leq z \leq 14$, membrane interval $-17 \leq z \leq 17$, and channel pore interval $-37 \leq z \leq 26$ in yellow, light-cyan, and green colors, respectively, to clearly display the distribution pattern of a 3D function in the z -axis direction, which coincides with the channel pore direction or a membrane normal direction.

Fig. 7 displays the distribution patterns of the electrostatic potential functions u^+ and u^- and concentration functions of K^+ , Na^+ , and Cl^- produced by the PNPSIC model in Tests 1 and 2. From Plots (a, b) it can be seen that there exist the strong positive and negative potentials u^+ and u^- within the selectivity filter range $2 \leq z \leq 14$ (in yellow color). Even so, as shown in Plots (c, d), the sodium and chloride ions have been prevented permeation from the filter while potassium ions transport through the filter across the membrane range $-17 \leq z \leq 17$ (in light-cyan color). This confirms that our PNPSIC model can

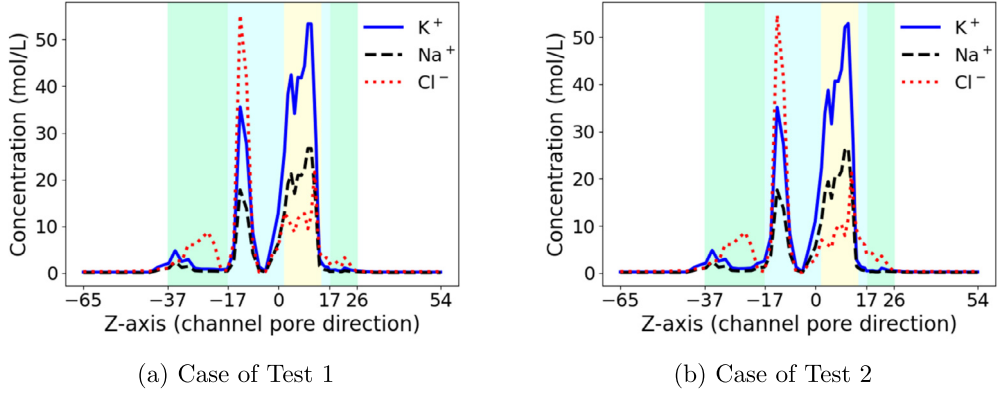


Fig. 8. Concentration functions of K^+ , Na^+ , and Cl^- produced by our PNPic model [2].

retain the ion selectivity property of a potassium channel. In addition, from a comparison of Test 1 results with Test 2 results we can see that boundary values and membrane surface charges can have a little affection on the concentration of potassium ions within the filter, implying that the molecular structure and atomic charges within the filter play a major role in the determination of potassium distribution profiles.

Fig. 8 displays the concentration functions generated by a current PNP ion channel (PNPic) finite element software package developed in our previous work [2]. Here we repeated Tests 1 and 2 using this package as a comparison of the PNPSIC model with the PNPic model. We do not report the potential functions u^- and u^+ generated by the PNPic package since they are found to have the distribution pattern similar to those given in Plots (a, b) of Fig. 7.

From Figs. 7 and 8 we can see that potassium ions dominate sodium ions over the solvent domain D_s , especially within the ion selectivity filter, since the bulk concentration of K^+ is double that of Na^+ (0.2 vs. 0.1 mol/L). This indicates that both PNPSIC and PNPic models retain one basic physical property — An ionic species having a larger bulk concentration can be stronger in competition for space among the species having the same charge number. We also can see that chloride ions become dominating within the cavity near the left side of the filter (about $-15 < z < -10$) since the bulk concentration of Cl^- is larger than the bulk concentrations of K^+ and Na^+ (0.3 vs. 0.2 and 0.1 mol/L). This indicates that both PNPSIC and PNPic models can retain another feature of a potassium channel — the cavity is filled with an ionic solution. However, from the PNPic prediction results reported in Fig. 8 it can be seen that both sodium and chloride ions have entered the filter, along with potassium ions, due to the strong negative and positive potentials u^- and u^+ within the filter. These prediction results contradict the ion selectivity property of a potassium channel. Hence, we should substitute the PNPic model with the PNPSIC model in the study of a potassium channel.

Remark. Note that the curves of Fig. 7 cannot be used to understand the Slotboom variable transformation formulas of (31) since they are plotted by the average values of potentials and concentrations. For example, u has a value around 3 in Fig. 7(b) while the concentration c_1 of potassium ions has a value around 70 in Fig. 7(d) near $z = 17$. Applying these two values to the formula $\bar{c}_1 = c_1 e^u$, we get a large value of \bar{c}_1 :

$$\bar{c}_1 = 70e^3 \approx 1405.98.$$

The above value is incorrect because the range of \bar{c}_1 is between 0 and 1 only in Test 2. Actually, the formula $\bar{c}_1 = c_1 e^u$ does not hold in the average values as shown below:

$$\int_B \bar{c}_1(\mathbf{r}) d\mathbf{r} = \int_B c_1(\mathbf{r}) e^{u(\mathbf{r})} d\mathbf{r} \neq \int_B c_1(\mathbf{r}) d\mathbf{r} \int_B e^{u(\mathbf{r})} d\mathbf{r},$$

where B is a block of a block partition of the solvent domain.

8. Electric current calculation and validation

One important application of a PNP ion channel model is to calculate the electric current I_S flowing over a cross-sectional surface, S , of an ion channel pore. In the current PNPic models (see [1–3,39] for examples), all the ions are supposed to be possible to enter the ion channel pore. Thus, for a mixture of n ionic species in D_s , I_S is usually estimated in the expression

$$I_S = -\frac{e_c N_A}{10^3} \sum_{i=1}^n Z_i D_{i,e}^f \int_S \left[\frac{\partial c_i(\mathbf{s})}{\partial z} + Z_i c_i(\mathbf{s}) \frac{\partial u(\mathbf{s})}{\partial z} \right] d\mathbf{s}, \quad (61)$$

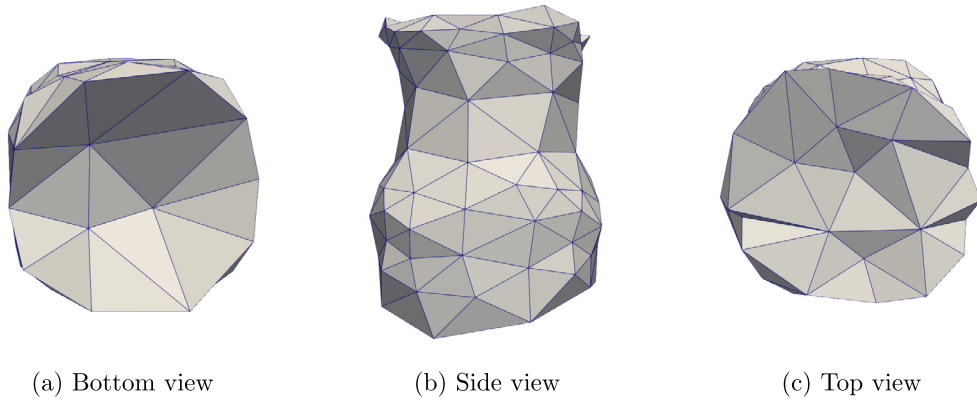


Fig. 9. A block B used in the formula (63) for electric current calculations.

where $\mathcal{D}_{i,e}^f$ and Z_i are the diffusion constant and charge number of Species i within the channel pore, respectively, I_S is measured in picoampere (pA; 1 pA = 10^{-12} ampere), and the normal direction of S coincides with the z -axis direction from the outside of a cell to the insider of the cell.

In the PNPSIC model, Species 1 is the unique species transporting ions across the membrane. Thus, we modify the formula (61) as

$$I_S = -\frac{e_c N_A}{10^3} Z_1 \mathcal{D}_1^f \int_S \left[\frac{\partial c_1(\mathbf{s})}{\partial z} + Z_1 c_1(\mathbf{s}) \frac{\partial u(\mathbf{s})}{\partial z} \right] ds.$$

To improve the numerical accuracy of computing electric current, following what is done in [1], we can approximate I_S as an averaged current, I_{ave} , using the volume integral

$$I_{ave} = -\frac{Z_1 e_c N_A}{h_B 10^3} \mathcal{D}_1^f \int_B \left[\frac{\partial c_1(\mathbf{r})}{\partial z} + Z_1 c_1(\mathbf{r}) \frac{\partial u(\mathbf{r})}{\partial z} \right] d\mathbf{r}, \quad (62)$$

where B is one block of the selectivity filter and h_B is the height of B in the z -axis direction. The above formula also avoids the difficulty of computing the related surface integral. To improve the numerical accuracy of computing partial derivatives $\frac{\partial c_1}{\partial z}$ and $\frac{\partial u}{\partial z}$, we use the first identity of (32) to reformulate the expression of I_{ave} as

$$I_{ave} = -\frac{Z_1 e_c N_A}{h_B 10^3} \mathcal{D}_1^f \int_B e^{-Z_1 u} \frac{\partial \bar{c}_1(\mathbf{r})}{\partial z} d\mathbf{r}, \quad (63)$$

where \bar{c}_1 is the Slotboom variable defined in (31), since \bar{c}_1 is smoother than both c_1 and u . We then calculate $\frac{\partial \bar{c}_1(\mathbf{r})}{\partial z}$ using the numerical techniques developed in our previous work [3] to further improve the numerical accuracy of computing electric currents. We implemented such a current computing scheme in Python as a part of our PNPSIC software package. We then calculated electric currents for the potassium channel and compared them with the experimental data reported in [34].

In our current calculation tests, the z -axis direction was set from the intracellular solvent domain $D_{s,l}$ to the extracellular solvent domain $D_{s,e}$, as illustrated in Fig. 1. The block B , as displayed in Fig. 9, was extracted from the selectivity filter mesh $D_{s,f,h}$ for $6 \leq z \leq 10$. Table 4 lists the eight values of voltage V and the corresponding values of the experimental electric current I_{exp} , which we extracted from one I-V curve reported in [34, Figure 2B] using the WebPlotDigitizer web server [40]. Table 4 also lists the predicted electric currents I_{pre1} , I_{pre2} , and I_{pre3} by the PNPSIC model, which we got, respectively, for the following three mixtures:

Mixture 1 100 mM KCl and 10 mM NaCl in $D_{s,l}$ and 100 mM KCl in $D_{s,e}$ for I_{pre1} .

Mixture 2 100 mM KCl and 50 mM NaCl in $D_{s,l}$ and 100 mM KCl in $D_{s,e}$ for I_{pre2} .

Mixture 3 100 mM KCl and 100 mM NaCl in $D_{s,l}$ and 100 mM KCl in $D_{s,e}$ for I_{pre3} .

In the above three mixtures, there are three ionic species (K^+ , Na^+ , and Cl^- ; i.e. $n_l = 3$) in $D_{s,l}$ and two ionic species (K^+ and Cl^- ; i.e. $n_e = 2$) in $D_{s,e}$. Here three different amounts of sodium ions are added to the intercellular solvent domain $D_{s,l}$, respectively.

In these tests, we set $\eta = 3$ and determined \mathcal{D}_1^f through fitting the values of I_{exp} in the case of Mixture 1. These values of \mathcal{D}_1^f were listed in Table 4 and applied to the calculation of I_{pre1} , I_{pre2} , and I_{pre3} . With cubic spline interpolation techniques

Table 4

Experimental current data (I_{exp}) extracted from [34, Figure 2B], three predicted current data (I_{pre1} , I_{pre2} , and I_{pre3}) by our PNPSIC model with the current formula (63), and the values of \mathcal{D}_1^f used in the calculation of I_{pre1} , I_{pre2} , and I_{pre3} . Here V is the voltage defined in (13) with $u_e = 0$ in millivolts (mV) and currents are in pA.

V	-100	-75	-50	-30	0	30	50	75	100
I_{exp}	-5.21	-4.10	-3.42	-2.60	0	2.99	4.76	6.28	6.76
I_{pre1}	-5.32	-4.03	-3.58	-2.63	0	2.81	4.78	6.32	6.80
I_{pre2}	-5.1	-3.85	-3.4	-2.49	0	2.69	4.47	5.75	5.68
I_{pre3}	-4.91	-3.69	-3.24	-2.36	0	2.57	4.20	5.24	4.69
\mathcal{D}_1^f	0.00686	0.00784	0.01176	0.01568	0.01078	0.02058	0.02254	0.02352	0.02744

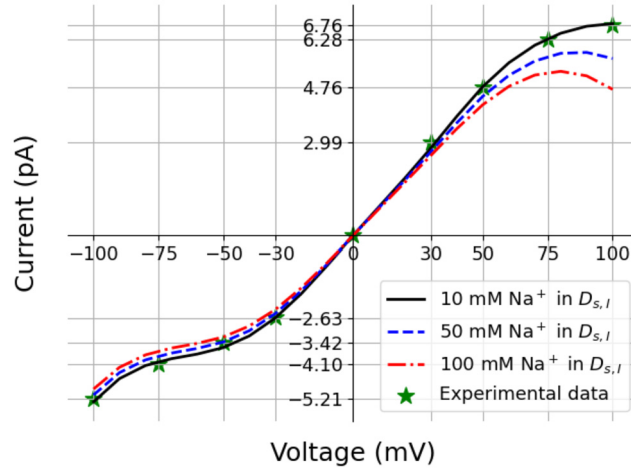


Fig. 10. Three I-V curves predicted by our PNPSIC model and a comparison with the experimental data [34, Figure 2B]. Here the solid, dash, and dot-dash curves are generated from the current data listed in Table 4 as cubic spline interpolation current functions for three mixtures of 100 millimolar (mM) KCl with 10, 50, and 100 mM NaCl in the intracellular solvent domain $D_{s,I}$, respectively, while 100 mM KCl is set in the extracellular solvent domain $D_{s,e}$.

and the data of Table 4, we constructed three I-V curves and displayed them in Fig. 10, along with a comparison with the experimental data report in [34, Figure 2B].

Fig. 10 shows that the PNPSIC model is able to produce electric currents close to experimental data. It also shows that the two predicted I-V curves in the case of Mixtures 2 and 3 can well retain the pattern of the I-V curve fitted by the experimental data in the case of Mixture 1. Moreover, from Fig. 10 we can see that the predicted currents are reduced, monotonically and significantly, with the increase of sodium ions in the intracellular solvent domain $D_{s,I}$. These test results agree with one characteristic of potassium channels – intracellular sodium ions can severely block the outward potassium ion flux through the selectivity filter, causing the reduction of outward potassium currents [33,34]. These test results further validate the PNPSIC model.

9. Conclusions

We have constructed the Poisson-Nernst-Planck single ion channel (PNPSIC) model based on a partition of a solvent domain, D_s , into an intracellular domain, $D_{s,I}$, an extracellular domain, $D_{s,e}$, and a selectivity filter domain, $D_{s,f}$, produced naturally from the ion selectivity property of a single channel protein. In the PNPSIC model, a concentration of a single ionic species is defined in the solvent domain D_s while two sets of ionic concentrations are introduced to describe the ion distribution profiles within $D_{s,I}$ and $D_{s,e}$, respectively. With this feature, the PNPSIC model can fully retain the ion selectivity property of a single channel protein. It also allows us to use different mixtures within $D_{s,I}$ and $D_{s,e}$ to mimic various biophysical experiments as is done in the electric current calculation in Section 8. In contrast, in current PNP ion channel models, all the ionic concentration functions are defined in the whole solvent domain D_s , causing that these current models do not work on any single channel and modifying them becomes very difficult.

However, our PNPSIC model is much more difficult to solve numerically than the current PNP ion channel models because it involves more unknown functions and more complex solvent domains. We have overcome these difficulties in this work through developing a new version of our current ion channel mesh generation package and an effective PNPSIC finite element solver. Moreover, we have implemented our PNPSIC finite element solver as a software package for a single ion channel protein with a three-dimensional X-ray crystallographic molecular structure and a mixture of multiple ionic species.

As one important application, we have introduced a new scheme for calculating an electric current flowing through the selectivity filter and validated our predicted I-V curves for a potassium channel by biophysical experimental data. Furthermore, numerical tests have been done for the potassium channel in a mixture of two different salts (sodium chloral and

potassium chloral), confirming the convergence and efficiency of our PNPSIC finite element solver and demonstrating the high performance of our PNPSIC software package.

It has been known that there are no water molecules in the selectivity filter of potassium [41]. Even so, we still follow the traditional PNP ion channel modeling approach to treat the filter region as a part of the solvent domain so that we can use a Poisson equation to fast calculate the electrostatic potential within the filter region. Although this simple treatment works in the calculation of electric current, as done in this work, it is attractive for us to substitute the Poisson equation (8d) with Coulomb, Lennard–Jones, or other potentials developed in molecular dynamics in line with the selectivity filter characteristic. Such a modification may significantly improve the quality of our PNPSIC model, especially in the calculation of an electrostatic potential within the filter region. We plan to do so in the future.

CRedit authorship contribution statement

- Zhen Chao: Mesh Software, Numerical Experiments, Figure Plotting, Reviewing and Discussions.
- Dexuan Xie: Methodology, Algorithms, Analysis, Software, Numerical Experiments, Writing and Editing, Supervision.

Declaration of competing interest

The authors declare that they have no known competing financial interests or personal relationships that could have appeared to influence the work reported in this paper.

Data availability

No data was used for the research described in the article.

Acknowledgements

This work was partially supported by the National Science Foundation, USA, through award number DMS-2153376 and the Simons Foundation, USA, through research award 711776.

References

- [1] D. Xie, B. Lu, Effective finite element iterative solver for a Poisson–Nernst–Planck ion channel model with periodic boundary conditions, *SIAM J. Sci. Comput.* 42 (6) (2020) B1490–B1516.
- [2] D. Xie, Z. Chao, A finite element iterative solver for an improved PNP ion channel model by Neumann boundary condition and membrane surface charge, *J. Comput. Phys.* 423 (2020) 109915.
- [3] Z. Chao, D. Xie, An improved Poisson–Nernst–Planck ion channel model and numerical studies on effects of boundary conditions, membrane charges, and bulk concentrations, *J. Comput. Chem.* 42 (27) (2021) 1929–1943.
- [4] Z. Chao, S. Gui, B. Lu, D. Xie, Efficient generation of membrane and solvent tetrahedral meshes for finite element ion channel calculation, *Int. J. Numer. Anal. Model.* 19 (6) (2022) 887–906.
- [5] D.A. Kelkar, A. Chattopadhyay, The gramicidin ion channel: a model membrane protein, *Biochim. Biophys. Acta (BBA), Biomembr.* 1768 (9) (2007) 2011–2025.
- [6] M. Colombini, The VDAC channel: molecular basis for selectivity, *Biochim. Biophys. Acta (BBA), Mol. Cell Res.* 1863 (10) (2016) 2498–2502.
- [7] B. Hille, *Ion Channels of Excitable Membranes*, Sinauer Associates, Sunderland, Massachusetts, 2001.
- [8] K.R. Rogers, M.A. Rogers, *Principles of Neural Science*, 2nd edition, Elsevier, New York, 1985.
- [9] K. Baker, D. Chen, W. Cai, Investigating the selectivity of KcsA channel by an image charge solvation method (ICSM) in molecular dynamics simulations, *Commun. Comput. Phys.* 19 (4) (2016) 927–943.
- [10] Z. Yao, B. Qiao, M.O. De La Cruz, Potassium ions in the cavity of a KcsA channel model, *Phys. Rev. E* 88 (6) (2013) 062712.
- [11] S. Berneche, B. Roux, Molecular dynamics of the KcsA K⁺ channel in a bilayer membrane, *Biophys. J.* 78 (6) (2000) 2900–2917.
- [12] C. Kutzner, H. Grubmüller, B.L. De Groot, U. Zachariae, Computational electrophysiology: the molecular dynamics of ion channel permeation and selectivity in atomistic detail, *Biophys. J.* 101 (4) (2011) 809–817.
- [13] I.H. Shrivastava, D.P. Tieleman, P.C. Biggin, M.S. Sansom, K⁺ versus Na⁺ ions in a K channel selectivity filter: a simulation study, *Biophys. J.* 83 (2) (2002) 633–645.
- [14] W. Kopec, B.S. Rothberg, B.L. de Groot, Molecular mechanism of a potassium channel gating through activation gate–selectivity filter coupling, *Nat. Commun.* 10 (1) (2019) 1–15.
- [15] C. Boiteux, D.J. Posson, T.W. Allen, C.M. Nimigeon, Selectivity filter ion binding affinity determines inactivation in a potassium channel, *Proc. Natl. Acad. Sci.* 117 (47) (2020) 29968–29978.
- [16] A. Burykin, M. Kato, A. Warshel, Exploring the origin of the ion selectivity of the KcsA potassium channel, *Proteins, Struct., Funct., Bioinform.* 52 (3) (2003) 412–426.
- [17] S.-H. Chung, B. Corry, Conduction properties of KcsA measured using Brownian dynamics with flexible carbonyl groups in the selectivity filter, *Biophys. J.* 93 (1) (2007) 44–53.
- [18] D.A. Doyle, J.M. Cabral, R.A. Pfuetzner, A. Kuo, J.M. Gulbis, S.L. Cohen, B.T. Chait, R. MacKinnon, The structure of the potassium channel: molecular basis of K⁺ conduction and selectivity, *Science* 280 (5360) (1998) 69–77.
- [19] Y. Zhou, J.H. Morais-Cabral, A. Kaufman, R. MacKinnon, Chemistry of ion coordination and hydration revealed by a K⁺ channel–Fab complex at 2.0 Å resolution, *Nature* 414 (6859) (2001) 43–48.
- [20] K. Zeth, U. Zachariae, Ten years of high resolution structural research on the voltage dependent anion channel (VDAC) – recent developments and future directions, *Front. Physiol.* 9 (2018) 108.
- [21] B. Honig, A. Nicholls, Classical electrostatics in biology and chemistry, *Science* 268 (1995) 1144–1149.
- [22] B. Roux, T. Simonson, Implicit solvent models, *Biophys. Chem.* 78 (1–2) (1999) 1–20.

- [23] B. Roux, Ion conduction and selectivity in K^+ channels, *Annu. Rev. Biophys. Biomol. Struct.* 34 (2005) 153–171.
- [24] B. Lu, Y. Zhou, Poisson-Nernst-Planck equations for simulating biomolecular diffusion-reaction processes II: size effects on ionic distributions and diffusion-reaction rates, *Biophys. J.* 100 (10) (2011) 2475–2485.
- [25] M.S. Kilic, M.Z. Bazant, A. Ajdari, Steric effects in the dynamics of electrolytes at large applied voltages. II. Modified Poisson-Nernst-Planck equations, *Phys. Rev. E* 75 (2) (2007) 021503.
- [26] J.-L. Liu, B. Eisenberg, Poisson-Nernst-Planck-Fermi theory for modeling biological ion channels, *J. Chem. Phys.* 141 (22) (2014) 22D532.
- [27] P. Liu, X. Ji, Z. Xu, Modified Poisson-Nernst-Planck model with accurate Coulomb correlation in variable media, *SIAM J. Appl. Math.* 78 (1) (2016).
- [28] J.-L. Liu, B. Eisenberg, Molecular mean-field theory of ionic solutions: a Poisson-Nernst-Planck-Bikerman model, *Entropy* 22 (5) (2020) 550.
- [29] D. Xie, An efficient finite element iterative method for solving a nonuniform size modified Poisson-Boltzmann ion channel model, *J. Comput. Phys.* 470 (2022) 111556.
- [30] D. Xie, S.H. Audi, R.K. Dash, A size modified Poisson-Boltzmann ion channel model in a solvent of multiple ionic species: application to VDAC, *J. Comput. Chem.* 41 (3) (2020) 218–231.
- [31] X. Liu, B. Lu, Incorporating Born solvation energy into the three-dimensional Poisson-Nernst-Planck model to study ion selectivity in KcsA K^+ channels, *Phys. Rev. E* 96 (6) (2017) 062416.
- [32] Z. Song, X. Cao, T.-L. Horng, H. Huang, Selectivity of the KcsA potassium channel: analysis and computation, *Phys. Rev. E* 100 (2) (2019) 022406.
- [33] R.J. French, J.B. Wells, Sodium ions as blocking agents and charge carriers in the potassium channel of the squid giant axon, *J. Gen. Physiol.* 70 (6) (1977) 707–724.
- [34] C.M. Nimigean, C. Miller, Na^+ block and permeation in a K^+ channel of known structure, *J. Gen. Physiol.* 120 (3) (2002) 323–335.
- [35] D. Xie, New solution decomposition and minimization schemes for Poisson-Boltzmann equation in calculation of biomolecular electrostatics, *J. Comput. Phys.* 275 (2014) 294–309.
- [36] R. Adams, J. Fournier, *Sobolev Spaces*, 2nd edition, Elsevier/Academic Press, Amsterdam, 2003.
- [37] L. Evans, *Partial Differential Equations*, Graduate Studies in Mathematics, vol. 19, American Mathematical Society, 1998.
- [38] A. Logg, K.-A. Mardal, G.N. Wells (Eds.), *Automated Solution of Differential Equations by the Finite Element Method*, Lecture Notes in Computational Science and Engineering, vol. 84, Springer Verlag, 2012.
- [39] B. Tu, M. Chen, Y. Xie, L. Zhang, B. Eisenberg, B. Lu, A parallel finite element simulator for ion transport through three-dimensional ion channel systems, *J. Comput. Chem.* 34 (2013) 2065–2078.
- [40] A. Rohatgi, Webplotdigitizer, version 4.6, <https://automeris.io/WebPlotDigitizer>, 2022.
- [41] C. Öster, K. Hendriks, W. Kopec, V. Chevelkov, C. Shi, D. Michl, S. Lange, H. Sun, B.L. de Groot, A. Lange, The conduction pathway of potassium channels is water free under physiological conditions, *Sci. Adv.* 5 (7) (2019) eaaw6756.